A Novel Experimental Approach for Curing Polymer Analysis

Andrew Byungkyu Kang

A thesis
submitted in partial fulfillment of the
requirements for the degree of

Master of Science in Aeronautics & Astronuatics

University of Washington

2019

Reading Committee:

Marco Salviato, Chair

Jinkyu Yang

Program Authorized to Offer Degree:
Aeronautics & Astronautics

University of Washington

Abstract

A Novel Experimental Approach for Curing Polymer Analysis

Andrew Byungkyu Kang

Chair of the Supervisory Committee:
Marco Salviato
Department of Aeronautics & Astronautics

In aerospace industry, understanding the development of stress within the composite part is a crucial aspect in producing high-quality composite parts. One such issue in composite manufacturing is the volume change of the polymer matrix material, that occurs as the epoxy cures and shrinks in volume. Over the years, several experimental procedures have been introduced to characterize various sources of this shrinkage. However, most of these methods are unable to provide an analysis of the epoxy throughout its cure cycle. In this paper, a novel experimental device is introduced to analyze the entire cure cycle of the matrix material of a typical composite. Unlike other previously proposed methods for curing polymer analysis, this apparatus aims to analyze the epoxy through rigorous stress calculation. Furthermore, it also aims to provide addition insights that may showcase relations between various cure characteristics that were previously unknown.

TABLE OF CONTENTS

LIST OF FIGURES

Figure Number Page

ACKNOWLEDGMENTS

The author wishes to express sincere appreciation to University of Washington, where he has had the opportunity to work with Professor Marco Salviato, Yao Qiao, and Eliot George who helped facilitate and guide this research towards success.

DEDICATION

for my father, who taught me to become the man I am today
my mother, who supported me through all my hardships and endeavors
and all my friends, for inspired me to push beyond my limits

Chapter 1
INTRODUCTION

1.1 Manufacturing of Composite Materials

The rapid transition towards the composite material in aerospace industry is driven by the numerous advantages they pose over traditional homogeneous materials. By combining two materials with drastically different characteristics, the resulting material becomes stronger and lighter than the individual parent materials. The history and advantages of composite material is well documented in Gibson's book [1]. One of the most popular material used in aerospace is the combination of carbon fiber with a polymer epoxy. The combination of the rigid filament and the light resin matrix has become one of the most utilized material in recent years. However, to maximize the performance of this material, many considerations need to be taken into its manufacturing procedure.

A typical manufacturing process of a composite part requires the use of an autoclave, which is a standardized industrial oven that subjects its specimen in a extreme temperature and pressure. This procedure sets the resin, accelerates the cure process, and removes any voids and air to further strengthen the finishing product. However, this means that the product will undergo volume change due to the high temperature change. Furthermore, due to the reactive nature of the epoxy, the matrix material of the composite will form cross-link and also experience chemical shrinkage. These effects will cause problem because the epoxy is also an adhesive that sticks to any surface it interacts with. A volume changing substance, that is restricted by another rigid structure, will tend to generate an internal stress. An example of this can be demonstrated in an FEA simulation of a thin shrinking plate, restricted on two ends.

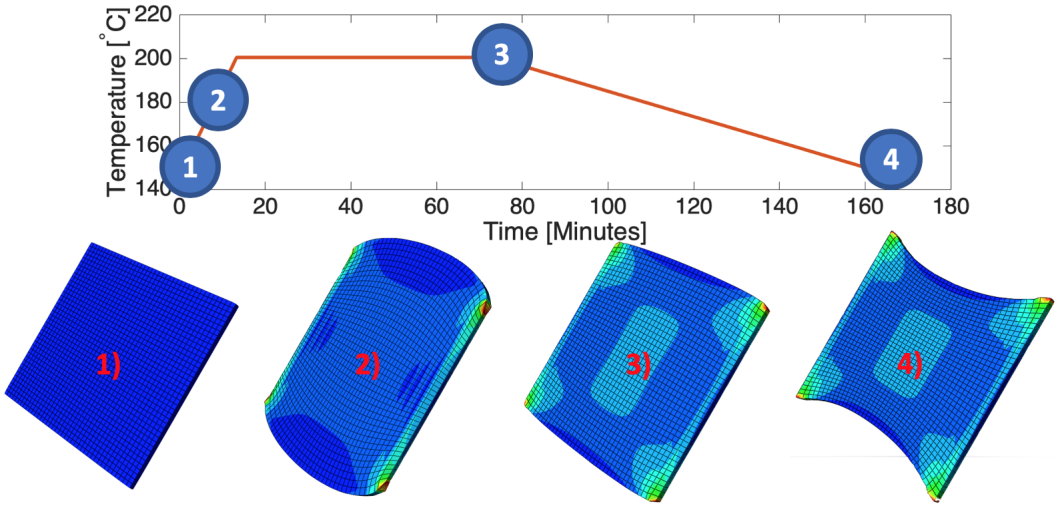

Figure 1.1: Volume Change of 8 mm Plate During Curing

This volume change can ultimately cause the final product to have undesirable deformations and imperfections, making the finishing product more prone to failure. This problem is especially pronounced for thicker composite parts, as thickness can create huge temperature gradient that can cause warmer region to cure faster. This could be problematic when manufacturing critical structural components, such as side stay fitting shown on figure 1.2. A thickness of a outboard lug (highlighted red on figure 1.2) can range between 60 to 68 mm [2]. To demonstrate the issue that can occur during the manufacturing, a finite element model of a composite plate with 60 mm thickness was subjected to a typical autoclave curing condition. The results showed that the highest temperature difference that a plate will experience during the cure process will be nearly 100 °F. Since the higher temperature accelerates the chemical reaction, high thermal gradient will lead to warmer part of the composite to cure faster than the colder region. This uneven curing process can cause the part to have cracks, which significantly reduces the life cycle of the part. In order to prevent such unwanted defects and other side effects, a thorough analysis of the cure behavior of the polymer epoxy is highly necessary.

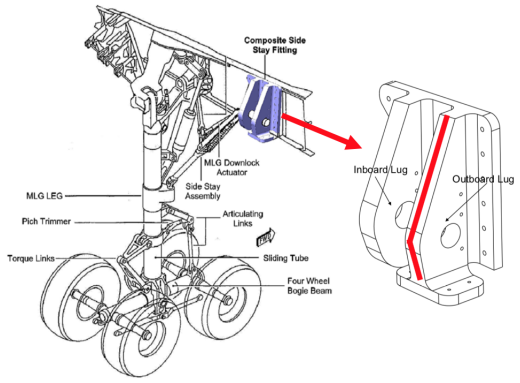

Figure 1.2: Typical Aircraft Landing Gear, and Side Stay Fitting [2]

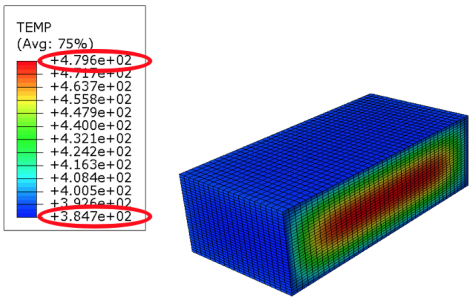

Figure 1.3: Largest Thermal Gradient of 60 mm Plate

1.2 Related Experimental Analysis

Over the years, various methods that have been developed to analyze the volume change of an epoxy will be showcased and discussed. Some of the earliest analysis of the epoxy mixture was done through the use of dilatometry technique, commonly used by chemists to determine the volume change of a mixture due to chemical or physical process [3]. These various techniques, specifically for curing epoxy, have been used all the way back since the 20th century.

There are numerous challenges in analyzing reactive polymers. One such problem is the tendency of the mixture to stick to any surface it interacts, which makes shrinkage

analysis difficult to achieve through direct contact. This means that quantity such as stress, which is important in material analysis, will require a novel and creative approach to be measured. Furthermore, the combined volume change from from temperature and chemical effect convolutes the process of determining the volume change of the epoxy. Finally, the material cross-links and changes the material property over time, which makes the analysis especially difficult to conduct.

There are many unique approaches for analyzing the curing epoxy. One experiment, conducted by Kravchenko *et al.*, used a digital image correlation (henceforth DIC) to analyze post-gel state epoxy mixture [4]. The use of DIC allowed them to avoid the sticking problem, while still being able to provide the in situ measurement of the specimen's strain. This simple method allowed them to determine the chemical shrinkage and coefficient of thermal expansion of the epoxy. However, this DIC method obtains these quantities using shear stress applied by the curing epoxy. Since the shear modulus of a pre-gel epoxy is almost zero, the shear stress applied by the mixture at an early stage is nearly undetectable through this method. This is seen on figures 1.5 and 1.6, where it shows that the experiment did not yield any results for degree of cure below 0.6. Thus, one of the major downside of this method is that it is unable to determine the chemical shrinkage prior to the gelation process of the mixture.

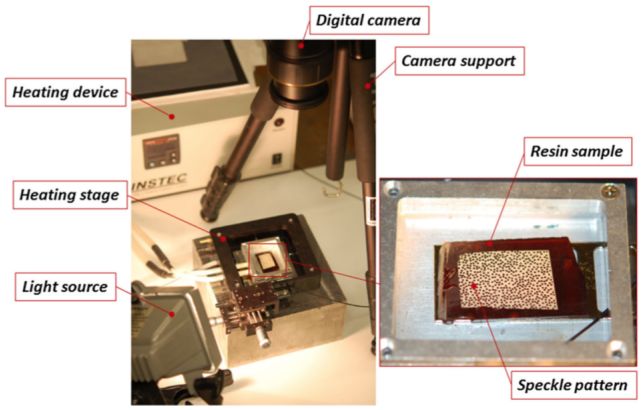

Figure 1.4: DIC Experimental Setup [4]

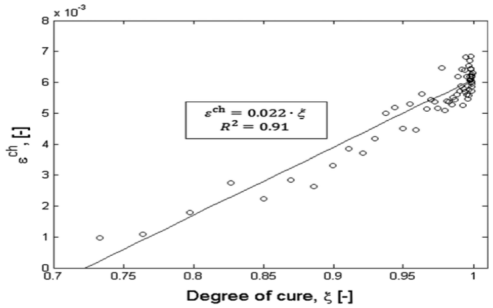

Figure 1.5: ϕ vs Chemical Shrinkage Coeff.

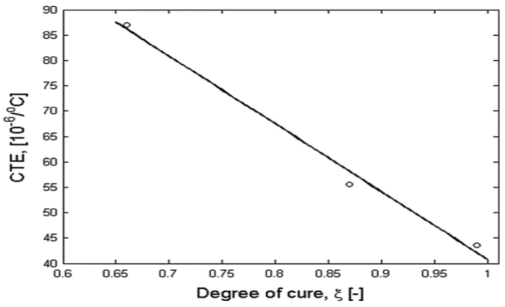

Figure 1.6: ϕ vs Thermal Expansion Coeff.

There are also other more complex methods that can analyze an entire cure behavior of the epoxy. In one study conducted by Nawab *et al.* [5], several cure dependent characteristics of an epoxy and heat transfer of the sample was determined by using an advanced PVT-α mould apparatus. This device allows the user to analyze the epoxy specimen under the effect of desired pressure and temperature. The device also allows the user to apply different temperature on separate regions of a specimen. This creates heat flux, which can enable the user to determine the thermal conductivity of the specimen using a guarded hot plate technique [6]. Another important characteristics that this apparatus can calculate is the bulk modulus of the epoxy. This quantity can be used in calculating the Young's modulus evolution of the epoxy.

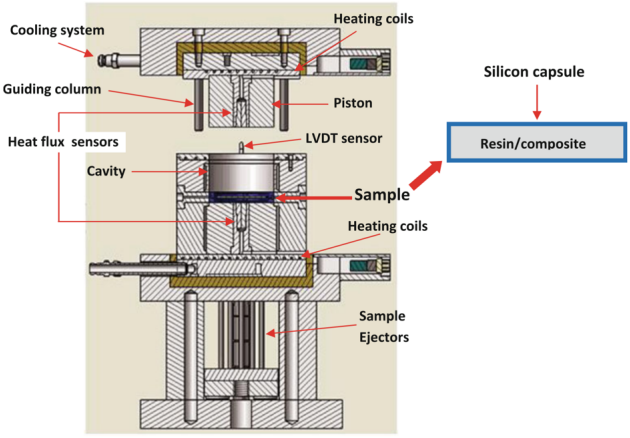

Figure 1.7: An Outline of PVT-α Mould Device [5]

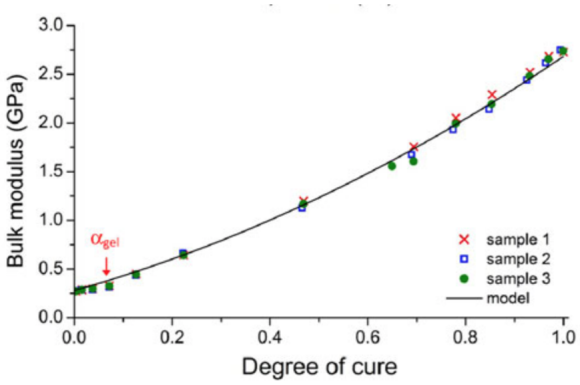

Figure 1.8: Bulk Modulus Evolution Obtained by PVT-α Mould [5]

$$E(\alpha) = E_1 + 3\alpha^2(1 - 2\nu) + \frac{\alpha E_2}{2} \tag{1.1}$$

Here, α is the bulk modulus, E_1 is the Young's modulus of neat resin, and E_2 is the Young's modulus of cured resin. However, in order to obtain the evolution of Young's modulus as a function of α, a Poisson's ratio must be determined. This can be achieved by taking direct stress measurement of the specimen. Unfortunately, this cannot be achieved for this method since the specimen under the analysis is encased within a silicone capsule.

1.3 Modeling Curing Behavior

Over the years, there have been several models that were introduced to predict the cure characteristics of an epoxy. In this section, some basic assumptions and models that are implemented widely in today's industry will be discussed and showcased.

1.3.1 Degree of Cure

Since curing of an epoxy mixture is an exothermic reaction, the mixture will generate heat over time. To characterize how much the mixture is cured, a concept of degree of cure is defined [7] as:

$$\phi(t) = \frac{H(t)}{H_r} \tag{1.2}$$

The degree of cure is defined by the amount of thermal energy released throughout its reaction. In equation 1.2, $H(t)$ is the heat generated by the mixture at the time t, and H_r is the total heat generated by the entire reaction. This means that the degree of cure value will increase over time, from 0 being uncured to 1 being completely cured. The relation between ϕ and time can be obtained through differential scanning calorimetry (henceforth DSC) device. If there are no physical data of the degree of cure behavior, it can also be approximated using a kinetics equation approximation. The approximation method will be discussed further in modelling in section.

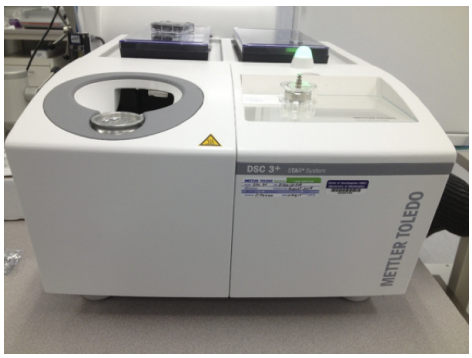

Figure 1.9: Differential Scanning Calorimetry Device

1.3.2 Model Validation via Curvature Comparison

As mentioned before, one of the most prevalent deformation that can reduce the life cycle of a composite part is the warpage from the volume change. One study aimed to use this warpage issue as an analysis component for characterizing one of the crucial quantities in epoxy analysis. In a model proposed by Chen and Zhang, [8], the curvature formed on a composite panel from warpage was used to directly correlate its residual stress. Although the model showed good correlation with experimental results, it is too simple and does not consider many other factors that contribute to the stress development during the cure. To truly analyze the development of the internal stress within part, more thorough and direct approach must be used.

1.4 Objective

While there are numerous methods that are proposed to study the cure behavior of an epoxy, many of them either fall short or are unable to provide the analysis of the entire cure cycle. The main objective of this paper is to introduce a novel experimental approach that can provide shrinkage analysis of an entire cure cycle of the epoxy. Typically, analyzing epoxy curing through direct stress measurement is avoided by most experimental methods due to many challenges it poses from sticking. The proposed device aims to take on this problem and provide a physical measurement of the stress development of the epoxy mixture throughout the entire cure cycle. The stress development will be compared with the results obtained from simulation to determine the reliability of the previously proposed models. The obtained data can also be used to characterize one of the key characteristic of epoxy analysis, chemical shrinkage.

Chapter 2

EXPERIMENTAL APPARATUS

2.1 Device Overview

The primary apparatus design is shown in figure 2.1 below. The primary structure of the device consists of two metal cylindrical walls, where the epoxy will be contained. The insides of the walls are covered using a plastic sheets, to prevent them from sticking to the epoxy. As the curing process continues, the shrinking epoxy will apply pressure onto these walls, causing them to deform. The wall deformation is measured using strain gauges. The strain gauges used in this experiment are linear strain gauges model SGD-1.5/350-LY13, from Omega Engineering. The measured analog data will be converted to a electrical signal using data acquisition board (henceforth DAQ), model NI-9219, from National Instruments Corporation. The base of the device consists of a ring shaped plastic plug, and a 3D printed stand that elevates the entire device. The purpose of the 3D printed base is to provide enough room for wires to connect the strain gauges to the DAQ.

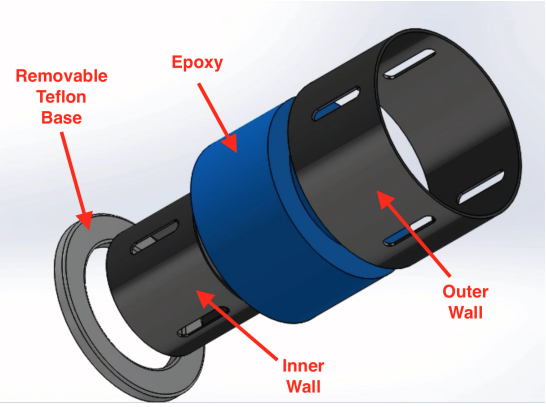

Figure 2.1: 3D Rendering of a Main Device

2.2 Cylinder Walls

The design for cylinder walls were chosen based on trial and errors involving both experimental, and simulation analyses. For the material of the cylinders, its linear elastic behavior has to be compliant enough to detect the shrinkage of the epoxy. Through finite element analysis (henceforth FEA), the ideal material for the wall was determined to be 6061 Aluminum. Beyond this, there were many other considerations that had to be made in order to design a viable apparatus that was both sensitive, yet structurally stable enough to withstand the shrinkage of the epoxy. The first consideration was the thickness of the cylinder, which plays crucial role in both the stability and sensitivity.

2.2.1 Wall thickness

In early design concepts, the walls of the cylinder were manufactured by cutting out various aluminum beverage cans. This was determined to be the easiest way to obtain the thinnest cylindrical aluminum specimen to be used for epoxy strain measurement. However, it was determined through FEA that these thin walls were highly susceptible to buckling under pressure, as seen in figure 2.3.

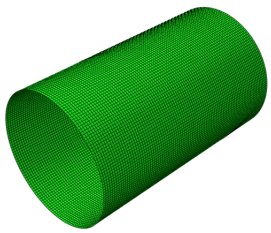

Figure 2.2: FEA Model of the Beverage Can

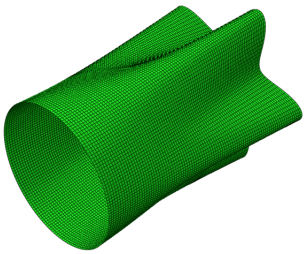

Figure 2.3: First Buckling Mode

Here, 0.1 kPa pressure was applied to the walls of a 250 ml energy drink can with a radius of 26.9 mm. The thickness of these cans are on average 0.1 mm, and the length of the cutout was set as 90 mm. Since the bottom of a device has to be sealed to contain

the epoxy, the bottom is assumed to be fixed from any movements. Thus, the one end of the cutout section was restricted from any displacements or rotations. The linear buckling analysis result showed that under such conditions, the can wall will be susceptible to the first buckling mode at around merely 9.724 kPa.

To avoid the buckling issue, the ideal thickness of the aluminum cylinder was set to be approximately 1 mm. To purchase 1 mm thick aluminum cylinder parts, the radius of the cylinder was determined around the available aluminum tubes with close to 1 mm thickness that could be purchased from the raw material manufacturers. Thus, two 3 feet long aluminum tubes were purchased from Mcmaster Carr - 0.049 inch thick tube with 3 inch diameter, and 0.035 inch thick tube with 2 inch diameter. The length of the wall was chosen to be 40 mm.

2.2.2 Amplifying Strain

Unfortunately, these thick walls were now too structurally stable to be deformed under the pressure applied by the curing epoxy. To improve the sensitivity, deliberate holes and other signal amplifiers were introduced to the wall surfaces. Various designs were tested using shell FEA analysis, such as 5 mm radius semi circlular hole (fig. 2.4), 8 mm wide and 5 mm deep notch (fig. 2.5), a 2.5 mm radius circular hole at the center (fig. 2.6), and a 20 mm long and 5 mm thick slot (fig. 2.7).

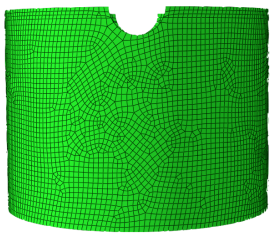

Figure 2.4: Semi-Circle at Top

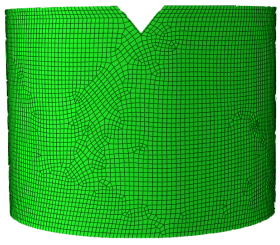

Figure 2.5: Notch at Top

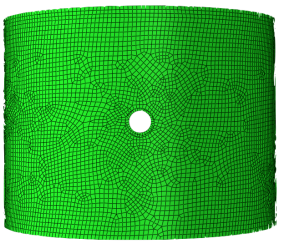

Figure 2.6: Circle at Center

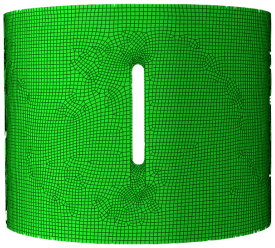

Figure 2.7: Slot

Similar to the buckling analysis, the bottom of the device was fixed from any deviation, and 0.1 kPa pressure was applied on the cylinder walls. However, due to the shrinkage of the epoxy over time, the pressure applied will not always be applied on the entire wall. Since the mixture can only shrink in height, the pressure applied on the wall will also decrease in height. In a later section, the height change for a 40 mm tall specimen was approximated to be around 2 mm. Taking this into account, a series of FEA tests were conducted on the four different models and the minimum tangential strain value was compared and tabulated:

Table 2.1: Minimum Tangential Strain Values

	Semi-Circle	Notch	Mid Hole	Slot
No Shrinkage	-2.495e-4	-2.314e-4	-1.442e-4	-6.443e-4
With Shrinkage	-1.564e-4	-1.324e-4	-1.440e-4	-6.503e-4

There are several things to note from these tests. The strain readings for the case with no shrinkage is higher for models with imperfections near the top of the rim of the model. This is not the case once the shrinkage is accounted, as the height change drastically affects the magnitude of compression for the semi-circle and notch models, as both experience nearly 60% decrease in compression. However, the hole at the center and the slot model does not experience such drop.

Considering these results, it was determined that the final design would have to accommodate for height change from the shrinkage, while still maintaining a good compression reading. Thus, the final hole design was chosen to be a long slot in the direction of the cylinder's height. Not only does this design have very high maximum compression (approximately -6.4e-4 with same conditions applied), the value is barely affected by the shrinkage.

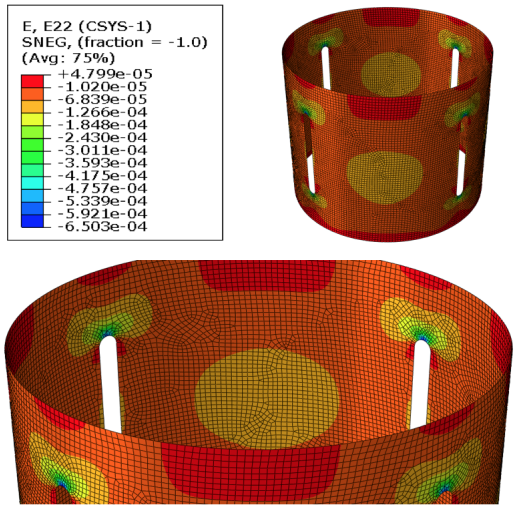

Figure 2.8: Final Amplifier Design

The final design of the cylinder wall has four evenly placed lengthwise slots. Their drawings are provided on figure 2.9.

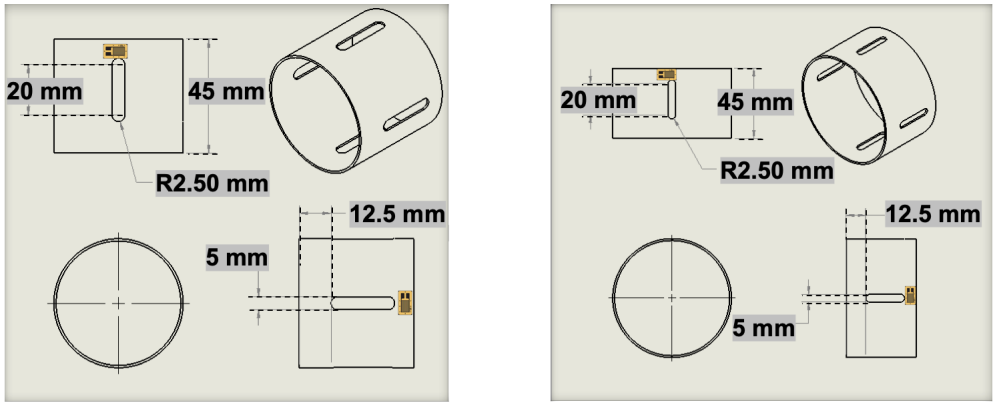

Figure 2.9: Wall Dimensions

2.2.3 Manufacturing Considerations

Today, metal tubes are formed by using a die casting procedure. However, this procedure leads to some internal stress to form within the tube, making them prone to unwanted deformation when cutting, or when shaving them down to thinner thickness using a lathe. Furthermore, adding four lengthwise slot to the parts made the cylinder walls even more challenging to manufacture into a desired dimension. The built in stress also restricts the length of the cylinder. Due to its tendency to deform after cutting, making a longer piece with a consistent radius throughout its length is very difficult. Overall, the dimension of the final product was selected, such that only a minimum alteration from the raw tube will be required.

2.3 Test Repeatability

As mentioned, the bottom of the device is a removable polymer ring plug that fits between the two aluminum walls, and the plastic sheet that lies in between them. This bottom ring is made out of polytetrafluoroethylene (specifically Teflon), which is a low-surface energy polymer that can prevent external materials from sticking to it.

The goal was to manufacture a plug that can provide a tight enough seal to keep the epoxy mixture from leaking during the curing. However, this proved to be very difficult since the plug also had to fit the two plastic sheets without causing any crumpling. Ultimately, the radii of the bottom plug was designed to be 0.011 inches off from the contacting cylinder walls, in order to ensure that the plastic wrapped around the walls of the cylinder smoothly. To prevent the leakage, high-temperature resistant tapes were used to seal the bottom after the plug and the plastic wrap were installed.

Shown on the left of figure 2.10 are two devices used for removal (called stamp and cavity on the figure). These were manufactured using a fused deposition modeling 3D printer.

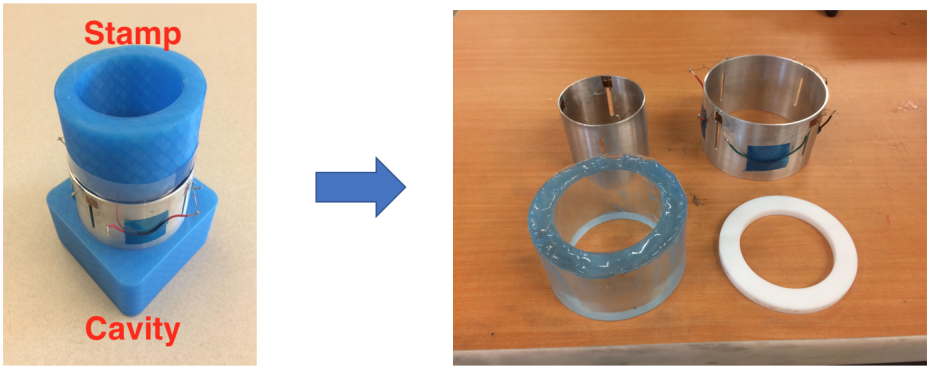

Figure 2.10: Removal of Cured Epoxy Demonstration

2.4 Data Acquisition

When it comes to taking measurement from the strain gauges, there are several options to configure them. The deformation of the aluminum wall is measured by detecting a very small change in resistance of the strain gauges. The sensitivity of the strain gauge to detect the deformation is determined by the concept of gauge factor, which is defined as shown below:

$$GF = \frac{\Delta R/R}{\Delta L/L} = \frac{\Delta R/R}{\varepsilon} \tag{2.1}$$

The change in resistance is usually very small, and requires a Wheatstone bridge circuit setup 2.11 in order to quantify into a usable signal:

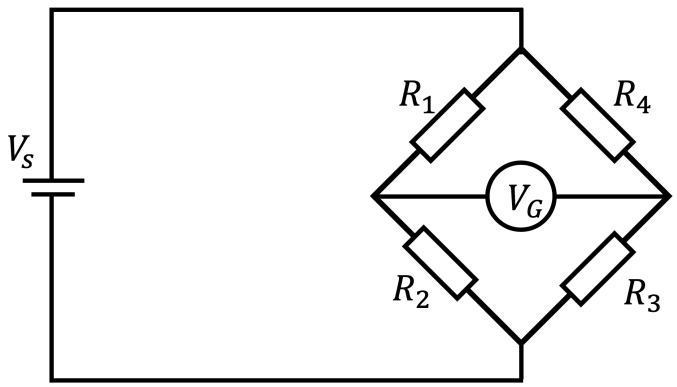

Figure 2.11: Wheatstone Bridge Circuit Diagram

Here, any perturbation of the resistance due to physical strain will cause the imbalance in the voltage reading across the bridge. The DAQ can take this incoming signal and filters it through the built-in signal conditioning circuitry. The filtered signal is then converted to a usable electrical signal, and will be logged onto a connected desktop computer to calculate the strain. The electrical signal recorded by the DAQ is the ratio of the galvanometer voltage V_G, and the supply voltage V_S.

The necessary circuitry setup for Wheatstone bridge is already done through the DAQ. The only requirement is to simply connect the gauges to the specified pin, and select the desired bridge configuration on the NI software. For this experiment, two different bridge configurations were explored for strain measurement:

2.4.1 Quarter Bridge

This set up only requires a single strain gauge to be connected. The main advantage of this setup is its simplicity, and convenience. However, this system is unreliable because a single gauge on its own is highly susceptible to the temperature change of the environment. This leads to a very noisy signal, and the results later will demonstrate the effect of ambient temperature change over several days. The relation between the strain and the voltage reading was found on the National Instrument's strain gauge measurement tutorial [9]:

$$\varepsilon_\theta = \frac{-4V_r}{GF(1+2V_r)} \tag{2.2}$$

$$V_r = \frac{\partial V_G}{V_S} \tag{2.3}$$

V_r is calculated by subtracting the first voltage ratio value from each recorded voltage ratio value. This allows the user to calculate the strain development of the specimen throughout the experiment time.

2.4.2 Full Bridge

In order to compensate for the effect of temperature change, a full bridge Wheatstone bridge setup can be utilized instead. This involves the use of 4 strain gauges where two gauges measure the tangential strain, while the other two serve to compensate for the temperature fluctuation. Referring back to figure 2.11, the voltage across the V_G can be determined using Kirchhoff's voltage law. The strain gauges measuring tangential strain will be installed adjacent to gauges that will read vertical strain. The vertical strain component will serve to compensate for the temperature.

$$V_G = V_s(\frac{R_1}{R_1 + R_4} + \frac{R_2}{R_2 + R_3}) \tag{2.4}$$

Then, applying perturbation theory, we determine the relation between the change in V_G, with the resistance change ∂R, assuming that supply voltage will remain constant.

$$\partial V_G = \frac{V_s}{4}(\frac{\partial R_1}{R_1} - \frac{\partial R_2}{R_2} + \frac{\partial R_3}{R_3} - \frac{\partial R_4}{R_4}) \tag{2.5}$$

Equation 2.5 was derived, assuming that same gauge is used for all 4 junctions and the the base resistance value are same. Referring back to the relationship between resistance and the strain measurement on equation 2.1, we can simplify the expression down into a relation between voltage measurement and strains. The relation between vertical strain and tangential strain was determined assuming isotropic relationship.

$$\partial V_G = \frac{V_s}{4} GF(\varepsilon_1 - \varepsilon_2 + \varepsilon_3 - \varepsilon_4) \tag{2.6a}$$

$$\varepsilon_\theta = -\nu\varepsilon_z \tag{2.6b}$$

$$\partial V_G = \frac{V_s}{4} GF(\varepsilon_\theta - \varepsilon_z + \varepsilon_\theta - \varepsilon_z) \tag{2.6c}$$

$$\frac{\partial V_G}{V_s} = V_r = \frac{GF}{2}(1 + \nu)\varepsilon_\theta \tag{2.6d}$$

$$\varepsilon_\theta = \frac{2V_r}{GF(1 + \nu)} \tag{2.6e}$$

2.4.3 Choosing Bridge Configuration

While the full bridge set up offers more stable measurement with temperature compensation, it requires a very careful and precise installation of strain gauges to be more effective than the quarter bridge. Ultimately, it was decided to use the quarter bridge set up for the experiments, due to its simplicity and lack of complication with the setup. For the tests, two strain gauges were used on each wall.

2.5 Installing Strain Gauges

For both cylinders, four linear strain gauges are installed on the surface that does not contact the epoxy mixture. These gauges are placed at the edge of the slot, where the largest strain reading was measured in FEA. Installing a strain gauge is broken down into two following procedures:

Surface Preparation

1. Begin preparing the surface by wiping it with acetone to degrease it.
2. Use 400-grit sand paper to abrade the surface of the cylinder wall.
3. Apply M-Prep Conditioner on the sanded surface, using a cotton tip applicator. This solution is an acid that will corrode any small metallic residue from the previous step.
4. Then, using a new cotton tip applicator, apply M-Prep Neutralizer 5A. This is an alkaline solution that stops the acid reaction. Wipe away the prepped surface using a clean paper towel.

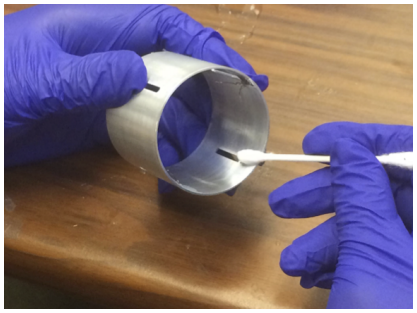

Figure 2.12: Using Cotton Tip Applicator

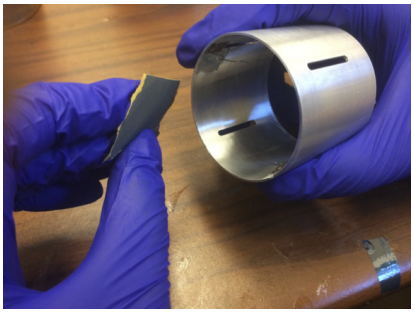

Figure 2.13: Abrading the Surface

Gauge Bonding

1. Take a strain gauge, and create a stress relief loop by using a toothpick.
2. Place the solder side down onto the adhesive side of a tape strip.
3. Place the tape on the surface such that the strain gauge is placed on the desired location.
4. Strip back just a portion of the tape so the non-solder side of the gauge is exposed for the catalyst and the adhesive to be applied.
5. Apply a catalyst onto the exposed surface, using the brush cap that comes with it.
6. Apply M-Bond 200 onto the surface, then place the tape back onto its original position. Apply a firm pressure on the surface to evenly coat the adhesive on the bottom surface of the gauge. Apply pressure for approximately 2-3 minutes.
7. Carefully remove the tape, at an angle. The gauge is now ready to be wired up.

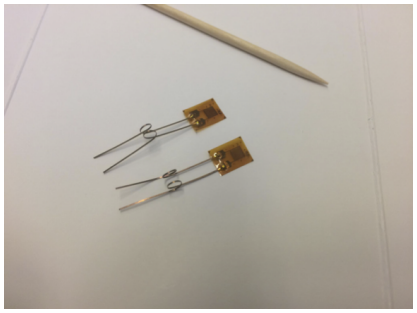

Figure 2.14: Strain Gauges w/ Relief Loops

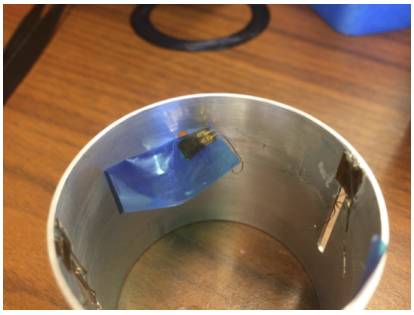

Figure 2.15: Exposed Gauge

2.6 3D Digital Image Correlation

The shrinkage is quantified by taking the current volume of the mixture, and dividing it by the original volume of the mixture. Since the mixture is only exposed on the top section of the device and is constrained between two walls, the shrinkage primarily occurs in the vertical direction. Thus, for this set-up, the volume shrinkage is equivalent to the height change % of the mixture. Incidentally, this height change % is also the vertical strain ε_z of the curing mixture. This value is necessary when calculating the Young's modulus evolution of the epoxy as it cures.

Although it is ideal to measure shrinkage in parallel with the strain on the wall, numerous tests have shown that the shrinkage behavior of the mixture is almost always consistent. Setting up two simultaneous tests were very difficult, due to the conflicting schedule of either apparatus that was used to measure strain and shrinkage. Thus, to resolve this conflict, shrinkage was measured separately by using a 3D printed replica of the device.

For the test set up, a thinly 3D printed sheet that matched the cross section of the device was coated with a speckle pattern, as shown on figure 2.16. Then, a dimensional replica of the device's aluminum walls were printed and covered with a plastic sheets. The epoxy was poured into the replica, and the speckled sheet was placed on top of the mixture. Using a 3D digital image correlation device (from Correlated Solutions Inc.), the movement of the speckle sheet in the vertical direction was captured. This motion was captured by using two adjacent cameras to detect the movement of a speckle pattern.

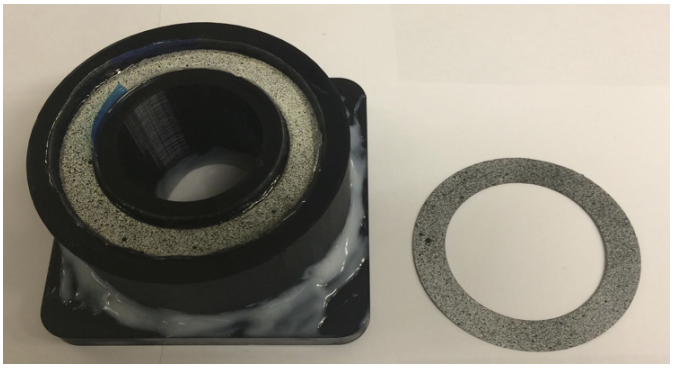

Figure 2.16: Device Replica & Speckle Sheet

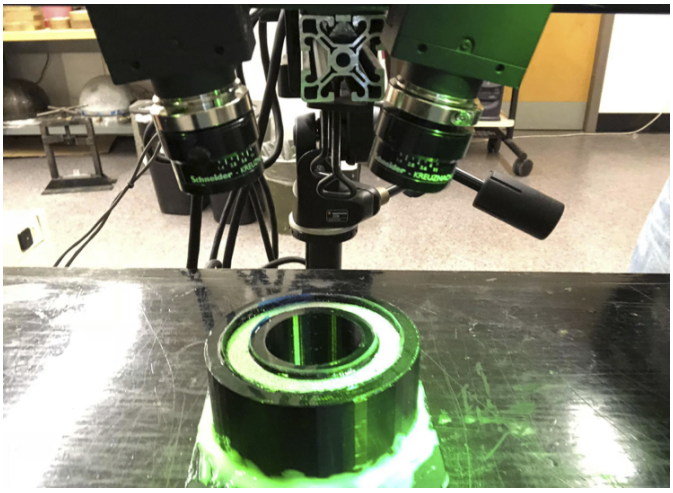

Figure 2.17: 3D DIC Two Camera Set Up

Chapter 3

EXPERIMENTAL RESULTS

3.1 Volume Shrinkage from DIC

As mentioned previously, the volume change was assumed to be only occurring in the z-direction. So to calculate shrinkage, change in height was divided by the original height of the specimen. The calculated value is also the total strain of the specimen in z direction. Thus, recorded volume change of the specimen was plotted against the degree of cure value. The degree of cure value for this experiment was obtained through kinetic equation approximation.

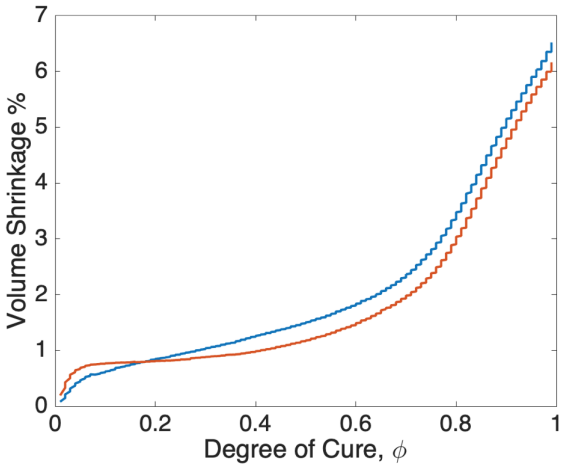

Figure 3.1: ϕ vs Volume Shrinkage of Two Tests

The result shows a bi-linear behavior of curing, where shrinkage occurs at slow and constant rate up till approximately 0.7 to 0.8 ϕ. However, the shrinkage rapidly increases near the end of cure cycle, beyond 0.8 ϕ. Higher rate of shrinkage near the end of cure cycle means that more rigid and cured epoxy is shrinking in volume. This could lead to higher stress development of the epoxy near the end of the cure cycle.

3.2 Strain Gauge Data

As explained in previous chapter, the obtained digital data was converted to tangential strain using eq. 2.2. Two strain gauges were attached on each walls, and their values were averaged for data fitting. In addition, a vertical line marking the time when the mixture reached full cure ($\phi = 1$) was added in as a purple dashed line for all obtained strain data.

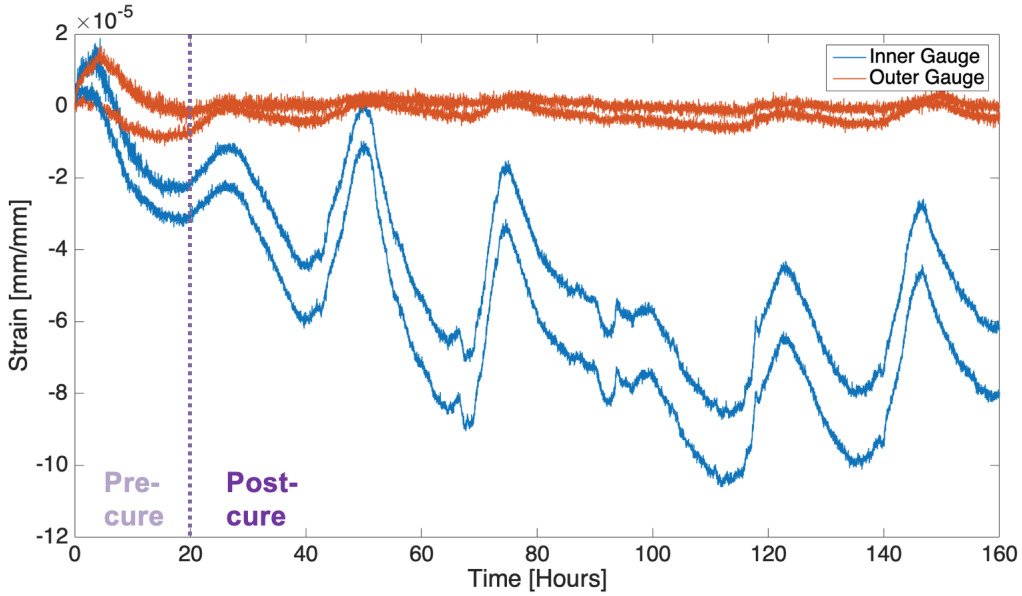

Figure 3.2: Obtained Strain Data

3.2.1 Stress on Outer Wall

The readings showed that the outer wall was barely able to detect any signal, with measured strain fluctuating below 10 μstrains. After the test, it was observed that the lack of signal was caused by the volume shrinkage of the mixture. As the epoxy shrank, it contracted away from the outer wall as shown on figure 3.3. Thus, the stress applied by epoxy on the outer wall was considered to be negligible.

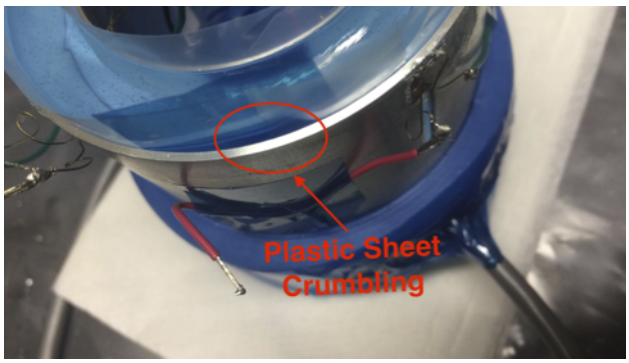

Figure 3.3: Effect of Shrinkage on Outer Wall

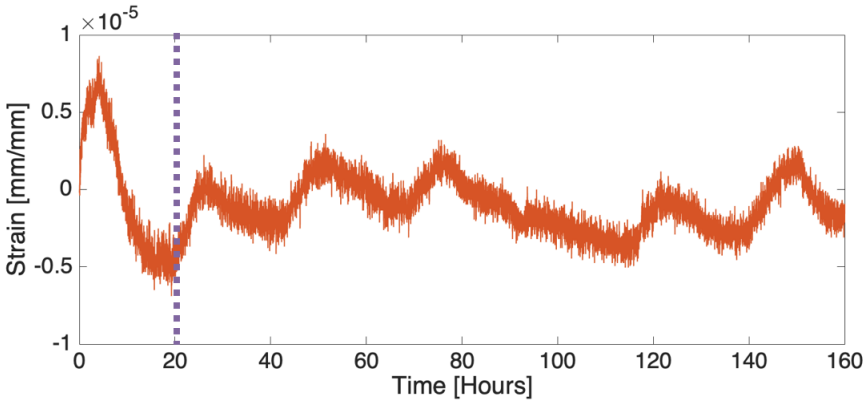

Figure 3.4: Avg. Outer Wall Strain Reading

3.2.2 Stress on Inner Wall

The obtained data had fluctuations that varied each day. This was concluded to be caused by the temperature change that happened due to day and night cycle. To compensate for such fluctuation, a polynomial fitting was done on the peak values to get a continuous non-oscillating behavior. Thus, the linear fits on figure 3.6 were obtained for inner and outer wall strain gauge data.

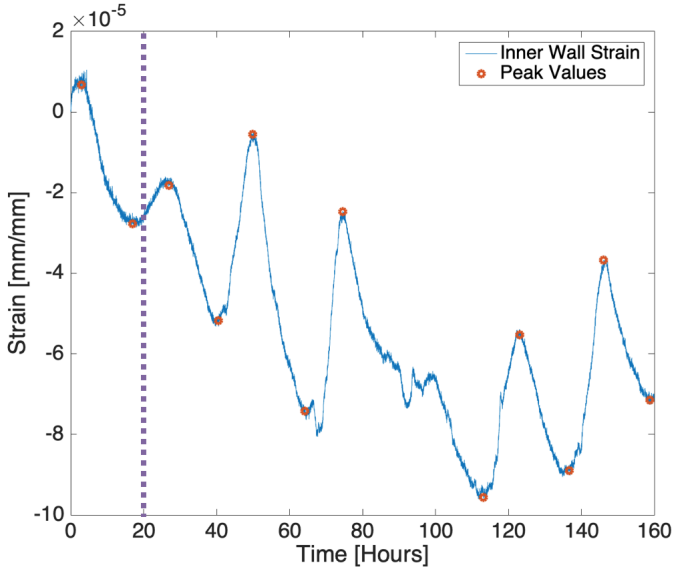

Figure 3.5: Avg. Inner Wall Strain Reading with Peak Values

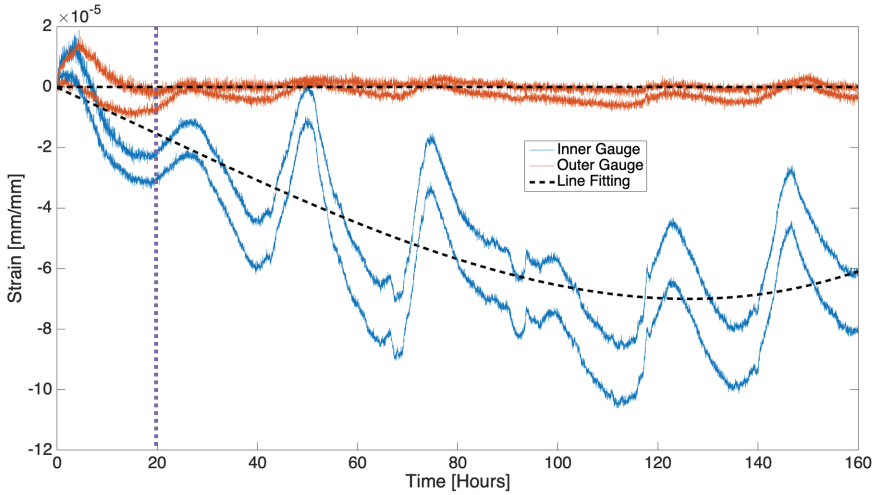

Figure 3.6: Total Strain Gauge Readings with Line Fitting

3.3 Finding Pressure using FEA

One of the important values that is required to conduct chemical shrinkage analysis is the pressure applied on the cylinder wall, by the curing epoxy. In previous section, it was observed that in room temperature, the outer wall will not exert any pressure due to shrinkage. However, this may not always be the case if the mixture experiences thermal expansion (henceforth TE) from large temperature change.

Since temperature was held at room temperature, only the pressure for the inner wall was needed to be calculated using the measured tangential strain from the experiment. To obtain the relation between the pressure on the contact surface of inner wall and measured strain, an FEA model of the inner ring was used.

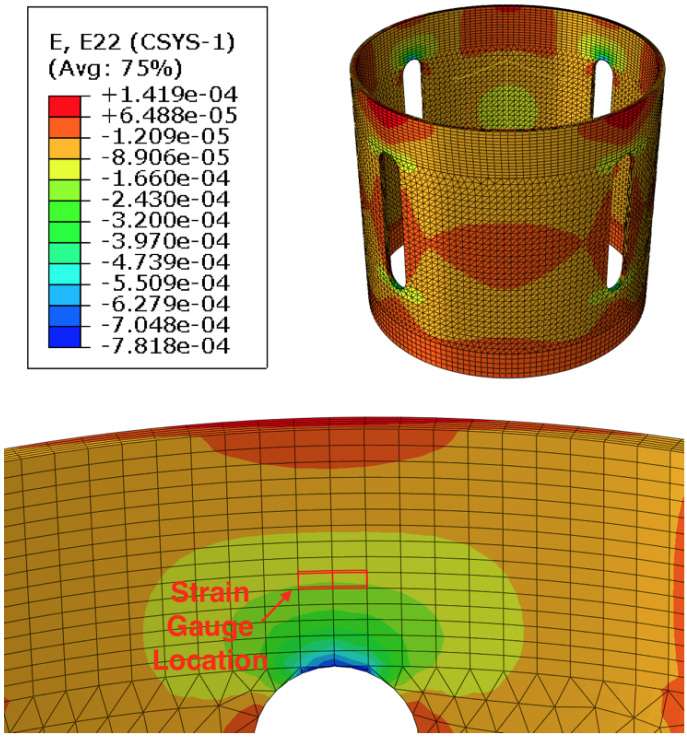

Figure 3.7: Calibration FEA Model

Since the strain gauge sensor is located 3 mm away from the tip of the slot (shown on figure 3.7), an element that is located at the same location was selected for analysis. The FEA result showed that the difference in strain between the model that accounted for shrinkage versus the one that did not was only around 5 to 6 μstrain. Therefore, the effect of shrinkage on strain was considered to be negligible.

Then, assuming linear relation between the applied pressure and the measured strain, a constant that will convert measured strain to pressure was be obtained. This constant will be referred to as C, and the fitted strain will be used to plot pressure against time and degree of cure, in the analysis and discussion chapter.

$$C = \frac{PressureApplied}{MeasuredStrain} \approx 609.76[MPa/strain] \tag{3.1}$$

Chapter 4

MODELING EXPERIMENT

4.1 Degree of Cure

To validate the results obtained from the experiments, the model provided by Heinrich *et al.* will be used [10]. To determine the cure kinetics of an epoxy, several theories are applied by the model. Overall, the curing process is modeled using a kinetic equation of a following form:

$$\frac{d\phi}{dt} = f(T,\phi) = (k_1(T) + k_2(T)\phi^m)(1-\phi)^n \tag{4.1a}$$

$$k_1(T) = A_1 \cdot exp(-\frac{\Delta E_1}{TR}) \tag{4.1b}$$

$$k_2(T) = A_2 \cdot exp(-\frac{\Delta E_2}{TR}) \tag{4.1c}$$

Equation 4.1b and 4.1c are Arrhenius equations, which are used to describe temperature dependence of various chemical reactions. ΔE refers to the activation energy, which is the amount of energy required for the reaction to occur. R is a gas constant, and constant A are pre-exponential factor that are determined through experiments. The constants m and n on the kinetic equation 4.1a, can be obtained through previously conducted experiments.

The kinetic equation can be used to approximate the degree of cure behavior of the mixture as a function of time. To check its reliability, ϕ obtained from equation 4.1a was compared with the actual ϕ obtained from DSC data. As shown on figure 4.1, ϕ behavior at various fixed temperature was determined for the type of epoxy used in this experiment.

The kinetic equation approximations shows that it could reliably predict the physical degree of cure behavior of an epoxy. Thus, equation 4.1a was used to find the relation between time and ϕ of the epoxy tested for the main stress development experiment of this paper. The test was conducted at room temperature, which was approximately 25 °C.

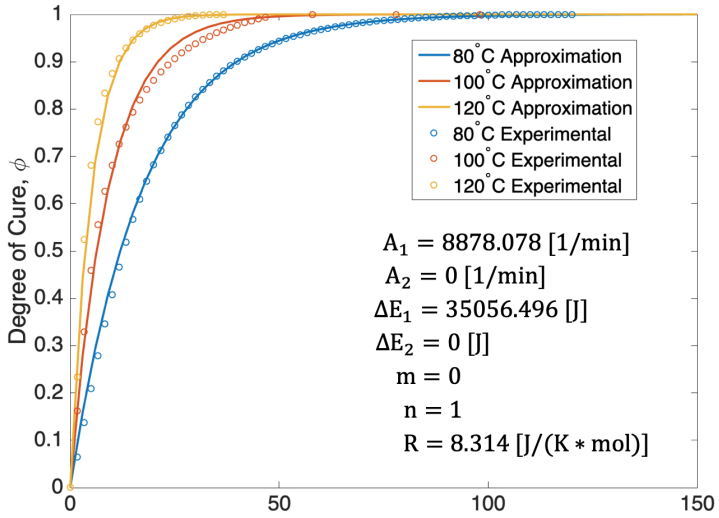

Figure 4.1: Degree of Cure Plots, with Kinetic Equation Parameters used in Approximation

4.2 Thermal Conductivity

Another characteristic that depend on the ϕ is a thermal conductivity of the material. The relation between the two values was determined by applying the local form of The First Law of Thermodynamics, and using equation 4.1a.

$$\rho c \frac{\partial T}{\partial t} = \frac{\partial}{\partial x_i}(\kappa(\phi, T)\frac{\partial T}{\partial x_i}) + \rho H_r \frac{\partial \phi}{\partial t} \tag{4.2}$$

Here, ρ is the current mass density of the mixture, c is the specific heat capacity, and κ is the thermal conductivity.

4.3 Network Modeling

To model the stress of curing epoxy, the network modeling method was utilized. The idea behind the model is to capture the behavior of a epoxy mixture that forms multiple cross link as it cures. Figure 4.2, shows an example of three cross-link network created at three different times. These networks occupy the same volume, and have different stress-free configurations. The sum of the stress states in all networks is such that the model balances out out all external forces applied on the volume of the specimen. The idea of formation of multiple networks that works in parallel, is the basis for modeling the stress behavior of a curing epoxy.

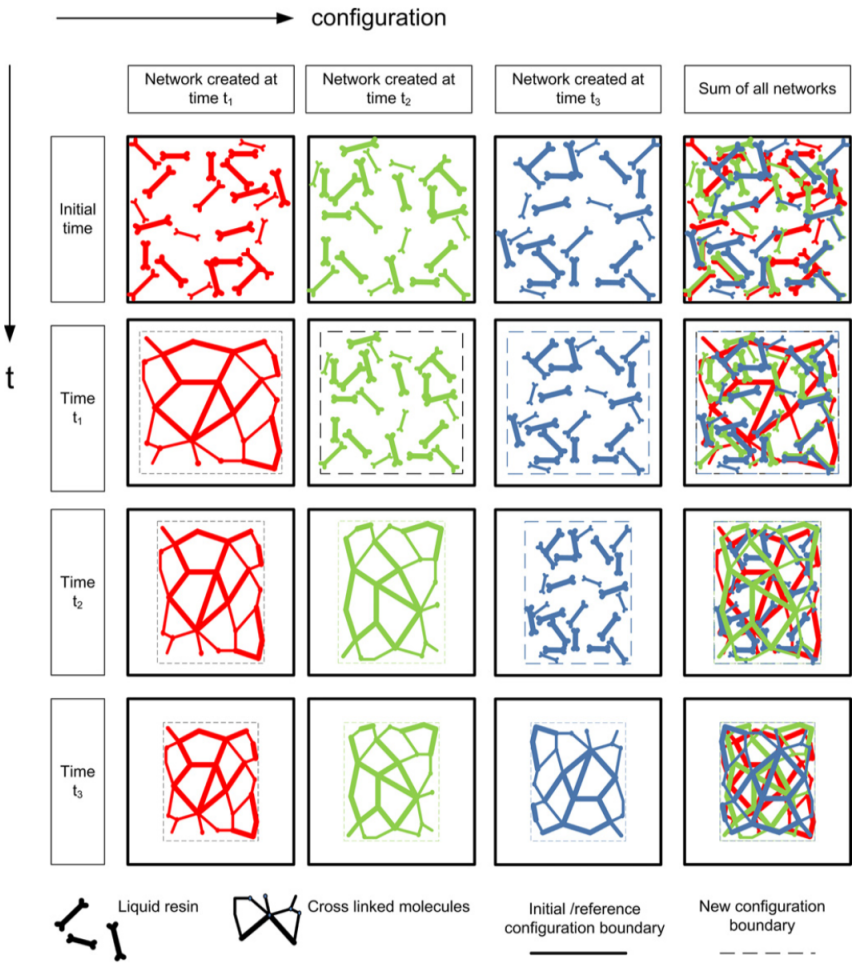

Figure 4.2: Formation of Cross-link Networks in Epoxy Specimen [11]

Traditionally, evolution of stress and the elastic properties are defined as a function of cure. Plepys, Vratsanos, and Farris [12, 13] propose to uses incremental elasticity to characterize this function. This meant that throughout the cure cycle, a linear elastic behavior could be assumed for a short period of time to describe the evolving material property. Assuming isotropic linear elastic property for the polymer, they were able use the stress and strain measured from the experiment to determine the material property throughout its cure, and correlate that with the cure rate of the epoxy.

Taking all these into consideration, a finite element code was developed from the study that can provide the comprehensive thermal/stress development history of curing epoxy. Using models and assumptions can help with predicting the epoxy's behavior. However, it is crucial to substantiate these claims using physical experiments.

4.4 Material Properties

To find the mechanical material property of the epoxy mixture, the model uses line fitting to approximate the two material properties, longitudinal modulus and shear modulus. These two values were approximated as a function of ϕ, using previously obtained experimental results. These experimental results are obtained through Raman and Brillouin light scattering [14], and are fitted onto the analytical function shown on equation 4.3b and 4.3a. The approximated material properties are used to determine the stress and strain, through incremental elasticity.

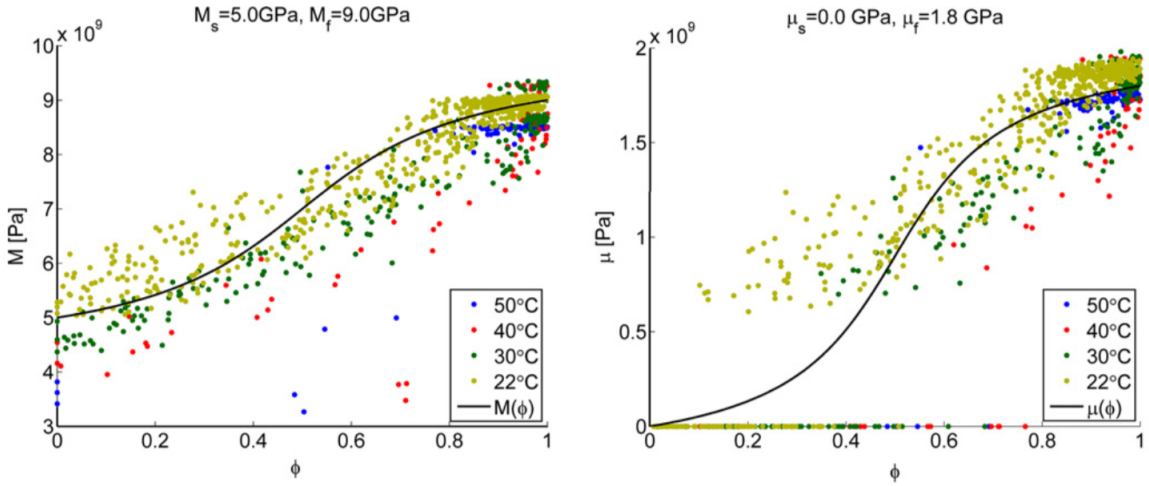

(a) Longitudinal modulus

(b) Shear modulus

Figure 4.3: Plots of Material Properties vs ϕ [10]

$$\mu_{tot}(\phi) = \frac{arctan((\phi - \frac{1}{2})\beta_\mu)}{arctan(\frac{\beta_\mu}{2})}(\mu_f - \mu_s) + \frac{\mu_f - \mu_s}{2} \tag{4.3a}$$

$$M_{tot}(\phi) = \frac{arctan((\phi - \frac{1}{2})\beta_M)}{arctan(\frac{\beta_M}{2})}(M_f - M_s) + \frac{M_f - M_s}{2} \tag{4.3b}$$

Chapter 5

ANALYSIS & DISCUSSION

5.1 Signal Fluctuation Analysis

It was mentioned in the previous chapter that the fluctuation of the obtained inner wall signal is most likely due to the ambient temperature change of the day and night cycle. To assess the temperature effect, an FEA simulation was used to determine the TE of the outer ring caused by the temperature change. Since the outer wall was separated from the shrinking epoxy, its experimental result can be used as a reference for the TE of just the aluminum wall.

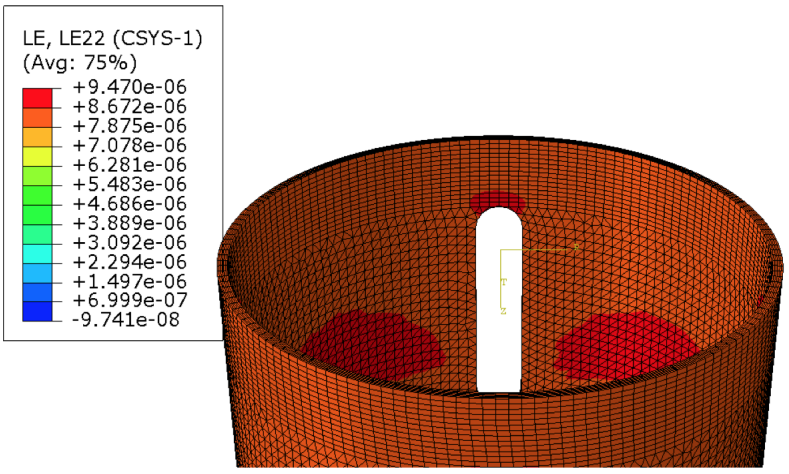

Figure 5.1: Thermal Expansion of Wall

Figure 5.1 is a TE result of the aluminum wall when it is exposed to a fluctuation between 19.5 °C and 20.5 °C at a period of 24 hours. From this it was noted that if an element is

sufficiently far away from the notch, the tangential strain value can be determined by using the basic linear TE relation (equation 5.1). Thus, dividing the outer wall strain by the coefficient of thermal expansion for aluminum ($\alpha_{T,al} = 2 \cdot 10^{-5} °C^{-1}$) results in a temperature fluctuation of the environment. Figure 5.2 shows that from the outer wall, the largest ambient temperature change is around 0.5 °C.

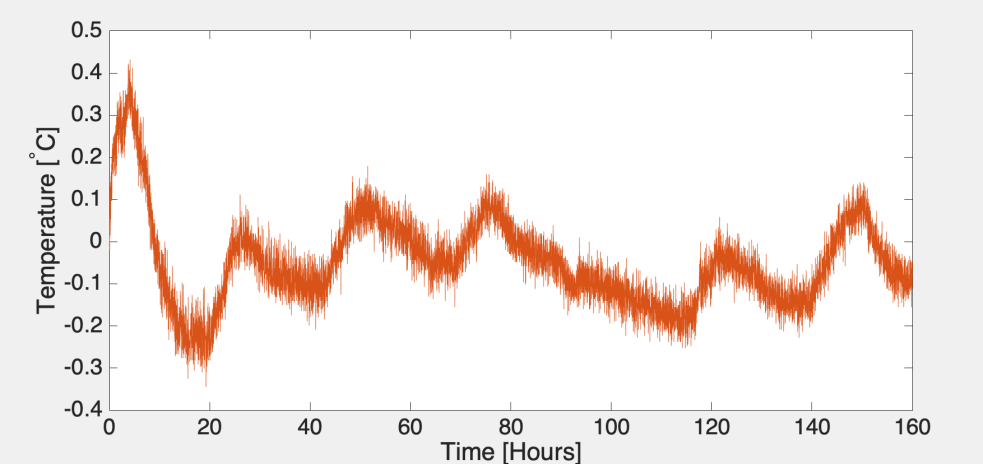

Figure 5.2: Average Experimental Outer Strain Converted to Ambient Temperature Change

$$\varepsilon_T = \alpha_T \Delta T \tag{5.1}$$

Compared to the outer wall, the inner wall experiences significantly larger strain oscillation. However, the inner wall is also making contact with the shrinking epoxy, which subjects it to the TE effect of the mixture. The coefficient of thermal expansion for cured epoxy ($\alpha_{T,ep} = 6 \cdot 10^{-5} °C^{-1}$) is larger than aluminum. The combined TE effect of the epoxy and the aluminum wall from 0.5 °C temperature change is determined by assuming linear thermal expansion for both materials:

$$\varepsilon_{T,tot} = \alpha_{T,ep} \Delta T - \alpha_{T,al} \Delta T = (0.5)(6 \cdot 10^{-5} - 2 \cdot 10^{-5}) = 2 \cdot 10^{-5} \tag{5.2}$$

Calculation of equation 5.2 analysis shows that assuming 0.5 °C temperature fluctuation, the inner wall should experience around 20 μstrains. However, figure 5.3 shows the amplitude

of the obtained inner strain signal is higher than the analysis result by an additional 20 μstrains. One explanation for this excess strain is due to one half of the aluminum wall being covered by the epoxy mixture. Since polymer epoxy has low thermal conductivity, the interface between the wall and polymer is likely to generate larger temperature change, which leads to more strain from TE. Thus, it is concluded that the signal fluctuation of the inner wall is greatly amplified by the fact that it is in contact with the cured epoxy mixture.

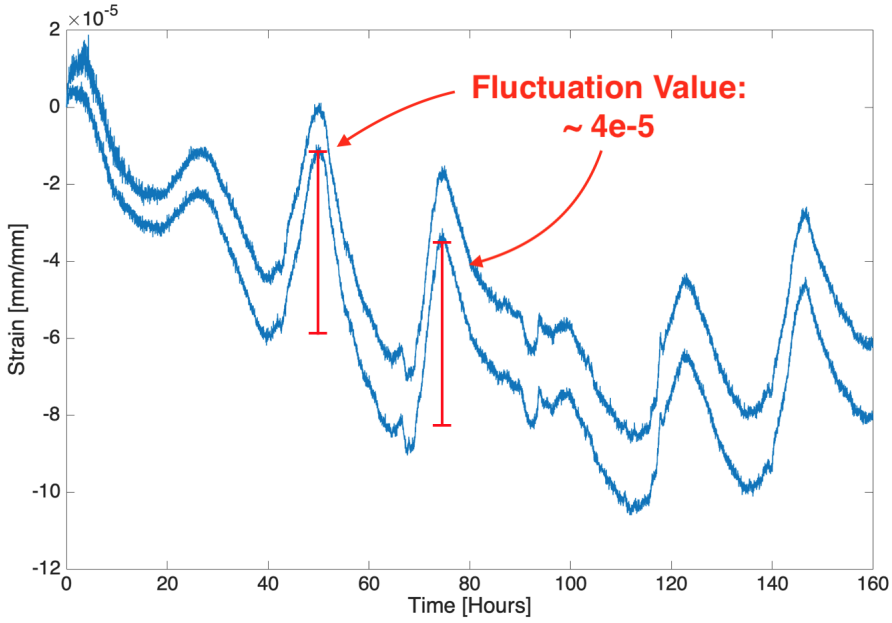

Figure 5.3: Inner Wall Fluctuation Values

5.2 Simulation Result Comparison

The test apparatus was replicated into an FEA model, in order to compare the strain generated within the model with the experimental results. The interface between the epoxy and the walls were assumed to be friction-less, and the bottom of the device was fixed from any displacement and rotation.

For comparison, the temperature was assumed to be constant for the simulation to replicate the ideal setting. Then, similar to what was done to the calibration model in section

3.1, the element that is located where the strain gauge sensor is place was used to compare the strain values.

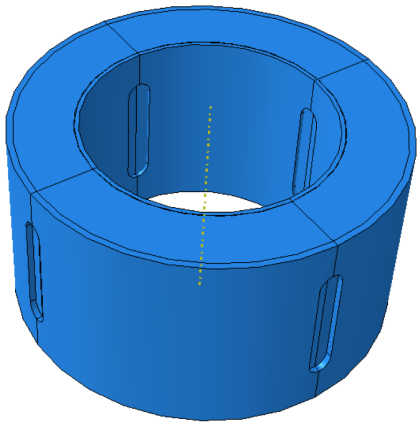

Figure 5.4: Shrinkage Analysis FEA Model

The obtained strain measurement will enable the comparison of all the values that were derived in the previous chapter. By simply applying the same procedure used on measured strain, the equivalent pressure value with respect to time and ϕ can be obtained for the simulated strain value as well. The obtained pressure from simulation was then compared with the results from the measured pressure.

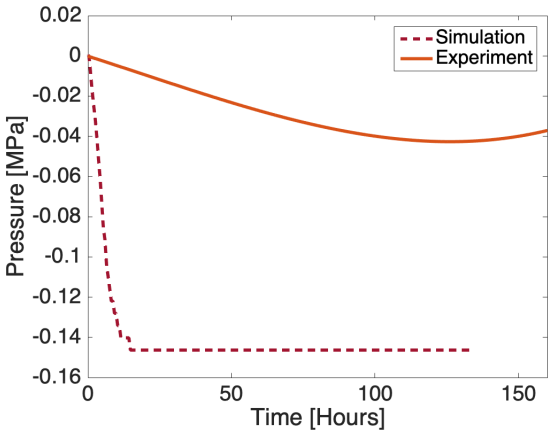

Figure 5.5: Pressure on Inner Wall vs Time

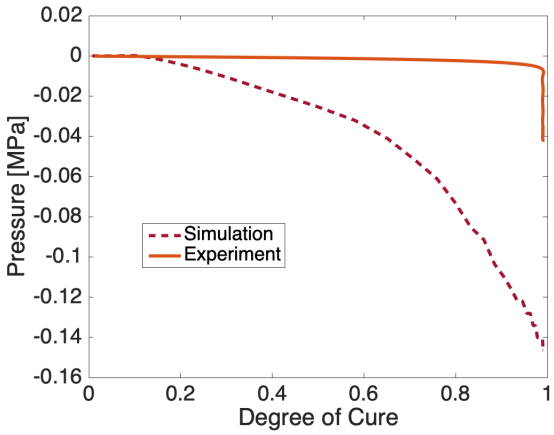

Figure 5.6: Pressure on Inner Wall vs ϕ

5.3 Experimental Pressure Results Discussion

The obtained results show that the simulated results estimate the pressure applied on the inner wall to develop much earlier than the experiment. Additionally, the stress development of the epoxy is shown to occur well after the mixture achieves full cure. As shown on figure 5.6, the degree of cure plotted against the pressure shows a very sharp asymptotic curve for the experimental result which indicates post-cure stress development behavior. While this is an unexpected result, it can be attributed to previously unaccounted viscoelastic quality of the mixture.

There are several possible reasons why the simulation results did not show late stress development. One possibility is that the kinetic equation used to predict the degree of cure is not accurately predicting the cure behavior of the mixture. In figure 4.1, the kinetic equation showed great correlation with the experimental results obtained for high constant temperature range (between 80 °C to 120 °C). It is possible that this accuracy may not hold for lower temperature. To confirm this, another DSC test must be conducted for the room temperature case.

Another likely explanation is the discrepancy between the material property predicted by the model and the actual material property from the experiment. While the simulation uses trigonometric functions to model the evolution of material property, this may not hold true for an actual experimental data.

5.4 Simulation Adjustment

As mentioned in an earlier section, the shrinkage results have shown that the majority of the volume change occurs near the end of the cure cycle. Considering this, it is logical to assume that an actual material property development also occurs mostly at the end of the curing cycle as well. Thus, the simulation code was altered to see if changing the material property will help it align more closely with the obtained results. Instead of using trigonometric approximations, a different fitting function was used to model the late shrinkage observed

from the result shown in figure 3.1. These were modeled using a natural exponential function, which seemed to better represent the delayed shrinkage effect than the tangential curve that inclines at 0.5 degree of cure.

The initial and final values of longitudinal and shear modulus (known values from experiments) were fitted onto a natural exponential function, shown in equation 5.3. The values A,B, and C are constants that are determined through fitting. The longitudinal modulus is assumed to increases from 1000 to 2500 MPa, while shear modulus goes from 0 to 925.93 MPa.

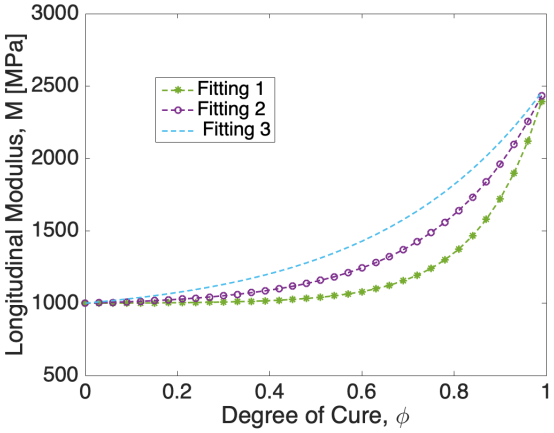

Figure 5.7: Longitudinal Modulus Fit

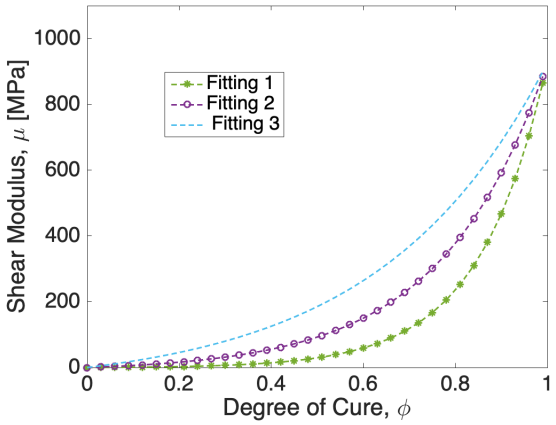

Figure 5.8: Shear Modulus Fit

$$f(\phi) = A \cdot exp(B\phi) + C \tag{5.3}$$

Table 5.1: M Fitting Constants

	A	B	C
Fitting 1	1	7.314	999
Fitting 2	18.75	4.394	981.3
Fitting 3	100	2.773	900

Table 5.2: μ Fitting Constants

	A	B	C
Fitting 1	1	6.832	-1
Fitting 2	11.57	4.394	-11.57
Fitting 3	61.73	2.773	-61.73

As shown in figure 5.7 and 5.8 fitting curves that approach the maximum modulus values at different rates were tested for comparison. Table 5.1 and 5.2 shows the fitting constants used for each curves. From these three new material property curves, three different simulations were ran. The tangential strain obtained from these simulations are presented alongside the experiment result.

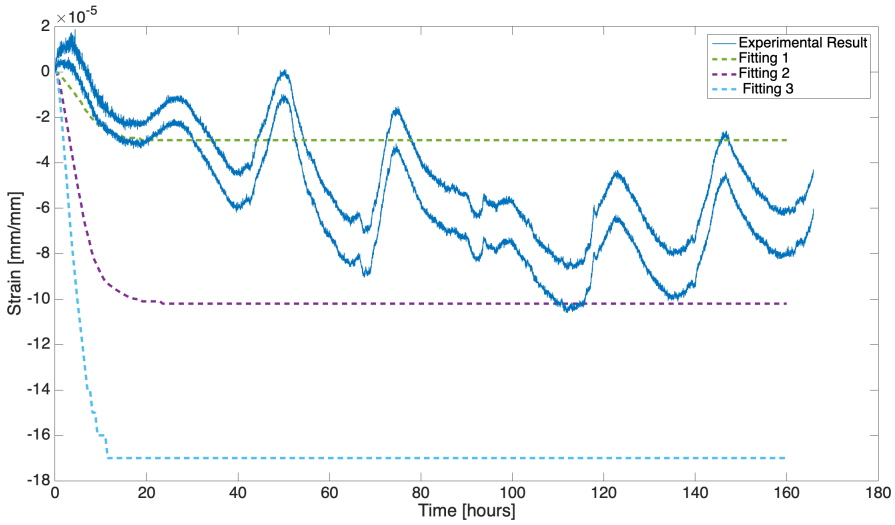

Figure 5.9: Simulation Strain Results vs Experiment Result

The three different estimations yielded have shown that the result approximated by the simulation will change drastically based on the evolution of the material property. Figure 5.9 shows three strain plots that plateau at different maximum strain values. It is observed that the simulation will estimate a higher strain, if the material property evolves at a faster rate.

Given such varied response from a subtle change in material property approximation, it is apparent that an improper characterization of material property evolution will lead to incorrect estimation of epoxy shrinkage behavior. In order for more reliable modelling, the material property evolution of the specimen must also be determined experimentally. This quantity can be obtained through further analysis, which will be discussed in the next chapter.

Chapter 6

FUTURE WORKS

6.1 Stress Components of Epoxy

The obtained pressure can be used to calculate the cylindrical stress components in the epoxy. Since the cured resin resembles the geometry of a thick cylinder, theory of thick shell can be applied in order to determine the stress components in terms of pressure applied on its side.

$$\sigma_r(r) = A - \frac{B}{r^2} \tag{6.1a}$$

$$\sigma_\theta(r) = A + \frac{B}{r^2} \tag{6.1b}$$

To obtain the unknown constants A and B, two boundary conditions must be applied - the pressure (equivalent to radial stress) applied by the outer wall and the pressure applied by the inner wall.

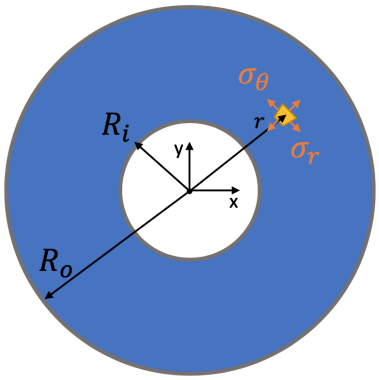

Figure 6.1: Cylindrical Stress Components of the Cured Epoxy

$$\sigma_\theta^p(R_o) = P_o = A + \frac{B}{R_o^2} \tag{6.2a}$$

$$\sigma_r^p(R_i) = P_i = A - \frac{B}{R_i^2} \tag{6.2b}$$

$$\sigma_r^p(r) = -P_o - \frac{P_i - P_o}{r^2}\frac{(R_i)^2(r - R_o)^2}{R_i^2 - R_o^2} \tag{6.2c}$$

$$\sigma_\theta^p(r) = -P_o - \frac{P_i - P_o}{r^2}\frac{(R_i)^2(r + R_o)^2}{R_i^2 - R_o^2} \tag{6.2d}$$

These stress equations are necessary in determining the Young's modulus evolution of the mixture.

6.2 Young's Modulus & Poisson's Ratio Evolution

The strain measured by the 3D DIC, and the strain gauge are total strains, and it can be divided into two components - mechanical and shrinkage strain.

$$\varepsilon_r^{p(tot)} = \varepsilon_r^{p(M)} + \varepsilon_r^{p(c)} \tag{6.3a}$$

$$\varepsilon_\theta^{p(tot)} = \varepsilon_\theta^{p(M)} + \varepsilon_\theta^{p(c)} \tag{6.3b}$$

$$\varepsilon_z^{p(tot)} = \varepsilon_z^{p(M)} + \varepsilon_z^{p(c)} \tag{6.3c}$$

Generally, the chemical shrinkage strain is obtained from other literature. In order to apply linear elastic theory on the epoxy, the mechanical strain must be used. Once it is calculated, Young's modulus and Poisson's ratio of the curing specimen can be derived through the use of Hooke's law and plane stress assumption. Like pressure, these values can be plotted as a function of degree of cure.

$$\varepsilon_\theta^{p(M)}(R_i) = \frac{1}{E(\phi)}(\sigma_\theta^p - \nu(\phi)\sigma_r^p) \tag{6.4a}$$

$$\varepsilon_z^{p(M)}(R_i) = -\frac{\nu(\phi)}{E(\phi)}(\sigma_\theta^p + \sigma_r^p) \tag{6.4b}$$

$$E(\phi) = \left(\frac{\varepsilon_\theta^{p(M)}(R_i)}{\sigma_\theta^p} - \frac{\sigma_r^p \varepsilon_z^{p(M)}(R_i)}{\sigma_\theta^p(\sigma_\theta^p + \sigma_r^p)}\right)^{-1} \tag{6.5a}$$

$$\nu(\phi) = \left(\frac{\sigma_r^{p(M)}}{\sigma_\theta^p} - \frac{\varepsilon_\theta^{p(M)}(R_i)(\sigma_\theta^p + \sigma_r^p)}{\varepsilon_z^{p(M)}(R_i)\sigma_\theta^p}\right)^{-1} \tag{6.5b}$$

6.3 Additional Analysis

Beyond just characterizing chemical shrinkage of an epoxy, the device used in the experiment can also be help with determining TE and cure degree gradient.

For future work, several more tests will have to be run at an environment where the temperature is no longer constant. This will introduce a third component to the total strain measured - thermal strain. Leveraging the elastic property information obtained from this test, the coefficient of thermal expansion can be determined using the similar approach that was used in chemical shrinkage analysis. This will allow full characterization of the coefficient of thermal expansion as a function of cure degree and temperature, which was never done previously in any literature.

The cure degree gradient will require a device with larger radius to impose a thermal gradient over the epoxy mixture. Majority of a traditional cure degree gradient analysis is conducted at the end of the cure cycle of an epoxy. In comparison, this device will allow the user to conduct real-time cure degree analysis of the entire cure cycle.

6.4 Design Improvements

To further improve the sensitivity of the strain signal, smaller strain gauges with lower resistance can be used instead. Figure 6.2 shows a comparison between the 350 Ω model used in experiment, and a smaller 120 Ω gauge. Since the lower resistance gauge is physically smaller, it can be placed closer to the edge of the slot and read even higher compression. Furthermore, a different Wheatstone bridge configuration (half-bridge or full-bridge) can be used to compensate for signal fluctuation to obtain more uniform results in future tests.

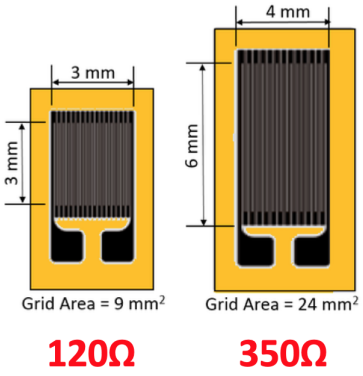

Figure 6.2: Strain Gauge Dimension [15]

In addition, an alternate method to measure the displacement in z-direction can be introduced to the design. The z-displacement can be measured through physical device such as linear variable differential transformer (LVDT) sensor. This sensor uses the metallic core that induces an electric and magnetic field, which can be directly correlated to the linear displacement measured by the sensor. Since the shrinkage occurs primarily in the z direction, the 3D DIC apparatus can be replaced with the LVDT. More importantly, this will also allow z-strain to be also measured in thermally controlled environment. This additional parameter will provide more leverage in determining coefficient of thermal expansion.

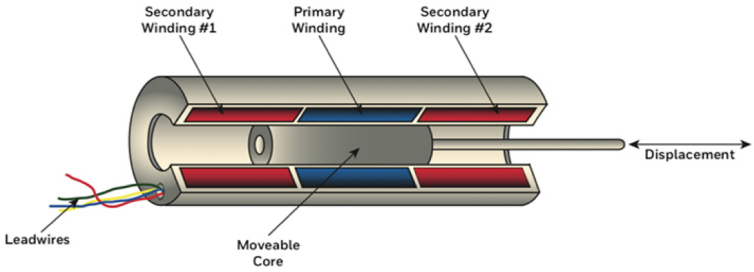

Figure 6.3: Basic LVDT Outline [16]

6.5 Physical Calibration Concept

In future test, it is ideal to determine the relation between the pressure on the aluminum wall and the strain through physical means. As seen on the result discussion section, simulation will not always accurately predict the strain value experienced by the specimen. To improve this, a separate calibration test must be ran on the device to determine the pressure value that corresponds to the strain reading from the strain gauge. This will help determine the exact value of the pressure applied by the shrinking epoxy.

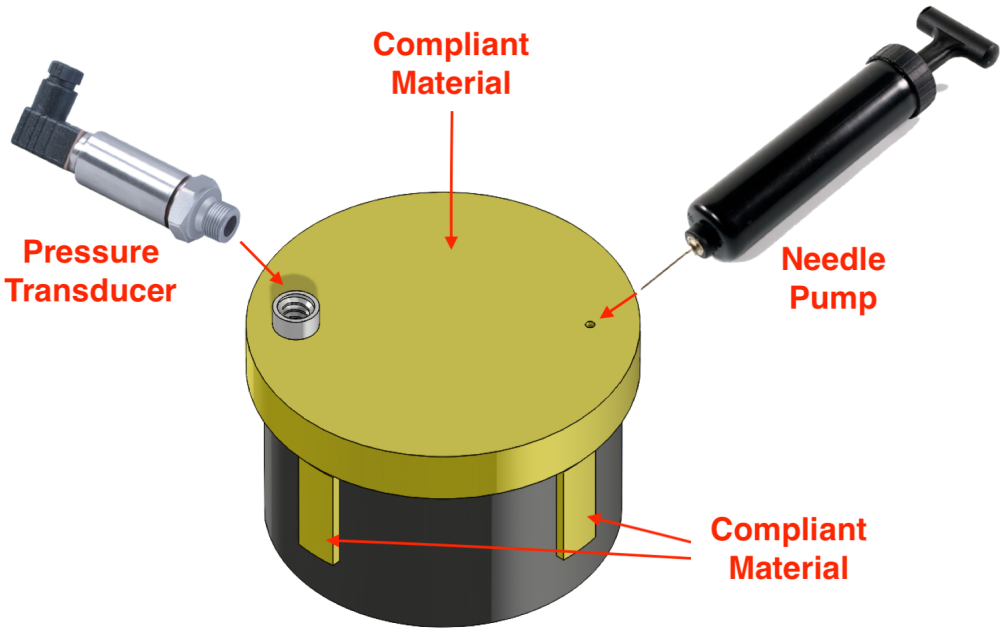

Figure 6.4: Calibration Device Concept

To apply pressure on the walls, the top section and the side slots will be sealed using an elastic material such as polyurethane or other forms of compliant polymer. The plug at the top will have two orifices - one for installing pressure transducer [17] and the other for pressurizing the sealed device using a needle pump. One possible way to manufacture such a plug is to use a PolyJet printer from Stratasys, Ltd., which enables the user to print hyper-elastic polymer parts for prototyping and testing [18].

Chapter 7

CONCLUSIONS

Through series of trial and error, a proposed idea for a epoxy analysis device was manufactured and refined. The most up to date design has achieved a nice compromise between the sensitivity required to measure strain from epoxy, while maintaining enough structural integrity to prevent unwanted deformation of the device. The results from the experiments have shown that the stress was developing well after the full cure was achieved. Compared to this, the simulation predicted that the stress will plateau once the mixture is fully cured. These have to be corroborated with additional experiments that provide consistent results. The obtained pressure value can be used to determine the Young's modulus development of the mixture experimentally. This additional step will be crucial in correcting the discrepancy of the results between the experiment and the simulation. Finally, with more improvements to the apparatus and additional analysis, this experimental work has the potential to discover many previously unknown properties and behavior of a curing polymer epoxy.

BIBLIOGRAPHY

[1] Richard F. Gibson. *Principles of Composite Material Mechanics*. CRC Press, 2012.

[2] K. Zimmermann, D. Zenkert, and M. Siemetzki. Testing and analysis of ultra thick composites. *Composites: Part B*, 41(4):326–336, 2010.

[3] Yasir Nawab, Salma Shahid, Nicolas Boyard, and Frdric Jacquemin. Chemical shrinkage characterization techniques for thermoset resins and associated composites. *Journal of Materials Science*, 48(16):5387–5309, 2013.

[4] Oleksandr G. Kravchenko, Segii G. Kravchenko, Aaron Casares, and R. Byron Pipes. Digital image correlation measurement of resin chemical and thermal shrinkage after gelation. *Journal of Materials Science*, 50(15):5244–5252, 2015.

[5] Yasir Nawab, Salma Shahid, Nicolas Boyard, and Frdric Jacquemin. Characterization of the cure shrinkage, reaction kinetics, bulk modulus and thermal conductivity of thermoset resin from a single experiment. *Journal of Materials Science*, 48:2394–2403, 2013.

[6] D. Salmon. Thermal conductivity of insulations using guarded hot plates, incluiding recent developments and sources of reference materials. *Measurement Science and Technology*, 12(12):R89, 2001.

[7] Kamal, M.R. Thermoset characterization for moldability analysis. *Polymer Engineering and Science*, 14(3):231–239, 1974.

[8] W. Chen and D. Zhang. A micromechanics-based processing model for predicting residual stress in fiber-reinforced polymer matrix composites. *Composite Structures*, 204(15): 153–166, 2018.

[9] National Instruments Corporation. Strain gauge measurement a tutorial. http://elektron.pol.lublin.pl/elekp/ap_notes/NI_AN078_Strain_Gauge_Meas.pdf. [Online; accessed 19-August-2019].

[10] Christian Heinrich, Michael Aldridge, Alan S. Wineman, John Kieffer, Anthony M. Waas, and Khaled W. Shahwan. Generation of heat and stress during the cure of polymers used in fiber composites. *International Journal of Engineering Science*, 53: 85–111, 2012.

[11] Y. Mei. *A stress evolution in a conductive adhesive during curing and cooling*. PhD thesis, Ann Arbor, Michigan: University of Michigan, 2000.

[12] A.R. Plepys, M.S. Vratsanos, and R.J. Farris. Determination of residual stresses using incremental linear elasticity. *Compsite Structures*, 27(1):51–56, 1994.

[13] A.R. Plepys and R.J. Farris. Evolution of residual stress in three-dimensionally constrained epoxy resins. *Polymer*, 31(10):1932–1936, 1990.

[14] K. E. Chike, M. L. Myrick, R. E. Lyon, and S. M. Angel. Raman and near-infrared studies of an epoxy resin. *Applied Spectroscopy*, 47(10):16311635, 1993.

[15] Siemens PLM Community. Strain gauges: Selecting an excitation voltage. https://community.plm.automation.siemens.com/t5/Testing-Knowledge-Base/Strain-Gauges-Selecting-an-Excitation-Voltage/ta-p/521034, 2019. [Online; accessed 12-August-2019].

[16] Motion Control Tips. Connex3 objet260 3d printer for multi-color multi-material models. https://www.stratasys.com/3d-printers/objet260-connex3. [Online; accessed 19-August-2019].

[17] Omega Engineering. Omega engineering. https://www.omega.com/en-us/sensors-and-sensing-equipment/pressure-and-strain/pressure-transducers/

p/PXM309?fbclid=IwAR1LKLf8DRqnfhZ3n-EVEVCE_lpm5DGKDqa2vE7YZ02aOitFb-B9Ofnn3sE. [Online; accessed 19-August-2019].

[18] Stratasys. What is an lvdt (linear variable differential transformer)? https://www.motioncontroltips.com/what-is-an-lvdt-linear-variable-differential-transformer/, 2018. [Online; accessed 12-August-2019].

[19] Issam Doghri. *Mechanics of Deformable Solids*. Berlin: Springer Verlag, 2000.

[20] Y. C. Fung. *First Course in Continuum Mechanics (3rd Edition)*. Englewood Cliffs: Prentence Hall, 1994.

[21] Naoto Ikegawa, Hiroyuki Hamada, and Zenichiro Maekawa. Effect of compression process on void behavior in structural resin transfer molding. *Polymer Engineering and Science*, 36(7):953962, 1996.

[22] MATLAB. *version 8.6.0.267246 (R2015a)*. The MathWorks Inc., Natick, Massachusetts, 2015.

Appendix A

MATLAB CODES

```
clear
clc
close all
%% Temperature

d = [0      146.2
     800 200.6
     4400 200.6
     10000 146.2];

figure(1)
plot(d(:,1)./60,d(:,2),'Color',[0.8500    0.3250    0.0980],'LineWidth',3)
set(gca,'FontSize',20)
xlabel('Time [Minutes]')
ylabel('Temperature [^{\circ}C]')


%% Area under curve test

dsc = csvread('dsc_res.csv',1,0);
t = dsc(:,1);
en = dsc(:,2);
```

```
area(t,en,'FaceColor',[0.3010 0.7450 0.9330]), hold on
area(t(1:1000),en(1:1000),'FaceColor',[0 0.4470 0.7410])
set(gca,'FontSize',20)
xlabel('Time [Minutes]')
ylabel('H [mW]')

%% Volume Shrinkage from DIC

shkg = csvread('volshrink.csv',1,0);
phi = shkg(:,1);
shr1 = shkg(:,2);
shr2 = shkg(:,3);


figure(4)

plot(phi,shr1,'LineWidth',2), hold on
plot(phi,shr2,'LineWidth',2)

set(gca,'FontSize',20)
xlabel('Degree of Cure, \phi')
ylabel('Volume Shrinkage %')


%% Kamal's Kinetic Model
```

```
kel = 273.15;                          % Kelvin constant conversion value
R = 8.314;                            % Gas Constant [J/(K*mol)]
E1 = 35056.493;                       % [J]
E2 = 0;
A1 = 8868.078;                        % ** Constant [1/min]
A2 = 0;                               % ** Constant [1/min]
T = 80 + kel;                        % Temperature
k1 = A1.*exp(-E1./T./R);
k2 = A2.*exp(-E2./T./R);

t = 0:3:150;
phi = 1- exp(-(k1+k2).*t);

figure(6)
plot(t,phi,'LineWidth',2), hold on



T = 100 + kel;                        % Temperature
k1 = A1.*exp(-E1./T./R);
k2 = A2.*exp(-E2./T./R);
phi = 1- exp(-(k1+k2).*t);

plot(t,phi,'LineWidth',2)


T = 120 + kel;                        % Temperature
k1 = A1.*exp(-E1./T./R);
```

```
k2 = A2.*exp(-E2./T./R);
phi = 1- exp(-(k1+k2).*t);

plot(t,phi,'LineWidth',2)


% DSC Results

dsc80 = csvread('dsc80d.csv',1,0);
dsc100 = csvread('dsc100d.csv',1,0);
dsc120 = csvread('dsc120d.csv',1,0);


plot(dsc80(1:100:end,1),dsc80(1:100:end,2),'o' ...
     ,'Color',[0    0.4470    0.7410]), hold on
plot(dsc100(1:100:end,1),dsc100(1:100:end,2),'o' ...
     ,'Color',[0.8500    0.3250    0.0980])
plot(dsc120(1:100:end,1),dsc120(1:100:end,2),'o'...
     ,'Color',[0.9290    0.6940    0.1250])

legend('80^{\circ}C Approximation','100^{\circ}C Approximation',...
       '120^{\circ}C Approximation','80^{\circ}C Experimental',...
        '100^{\circ}C Experimental','120^{\circ}C Experimental')
set(gca,'FontSize',20)
xlabel('Time [Minutes]')
ylabel('Degree of Cure, \phi')
```

```
%% Test from 07/19 QUARTER BRIDGE TESTS

vol0719 = csvread('NewSlotTest07192019.csv',1,0)./1000;

v = 0.33;                              % Poisson's Ratio
ti = 0.9;                              % Thickness [mm]
to = 1.25;
K = 2.06;                               % Gauge Factor

stq1 = -4.*vol0719(:,1)./K./(1+2.*vol0719(:,1));   % Strain Quarter Bridge
stq2 = -4.*vol0719(:,2)./K./(1+2.*vol0719(:,2));   % Strain Quarter Bridge
stq3 = -4.*vol0719(:,3)./K./(1+2.*vol0719(:,3));   % Strain Quarter Bridge
stq4 = -4.*vol0719(:,4)./K./(1+2.*vol0719(:,4));   % Strain Quarter Bridge

time0719 = (1:length(vol0719(:,1)));

figure(2)
plot(time0719./60,stq1,'Color',[0    0.4470    0.7410],'LineWidth',1), hold on
plot(time0719./60,stq3,'Color',[0.8500    0.3250    0.0980],'LineWidth',1)

plot(time0719./60,stq2,'Color',[0    0.4470    0.7410],'LineWidth',1)
plot(time0719./60,stq4,'Color',[0.8500    0.3250    0.0980],'LineWidth',1)

legend('Inner Gauge','Outer Gauge')
set(gca,'FontSize',20)
xlabel('Time [Hours]')
ylabel('Strain [mm/mm]')
```

```
xlim([0 160])

%% Average Graph

figure(11)
plot(time0719./60,(stq1+stq2)./2,'Color',...
     [0    0.4470    0.7410],'LineWidth',1)

set(gca,'FontSize',20)
xlabel('Time [Hours]')
ylabel('Strain [mm/mm]')


figure(12)
plot(time0719./60,(stq3+stq4)./2,'Color',...
     [0.8500    0.3250    0.0980],'LineWidth',1)

set(gca,'FontSize',20)
xlabel('Time [Hours]')
ylabel('Strain [mm/mm]')
xlim([0 160])



%% Shrinkage Data

shr = csvread('shrinkage.csv',1,0);
h = 40;                                          % Specimen height
```

```
zstr = -(shr(:,1)+ shr(:,2))./size(shr,2)./100./2;      % Z-strain
zstr = zstr.';


%% Filtering 2.0

stqin_av = (stq1+stq2)./2;


peakv = [176, 6.699e-6
         1016 -2.767e-5
         1613 -1.825e-5
         2426 -5.174e-5
         2990 -5.534e-6
         3853 -7.427e-5
         4478 -2.476e-5
         6791 -9.562e-5
         7385 -5.534e-5
         8203 -8.902e-5
         8767 -3.67e-5
         9526 -7.145e-5];

pfilt = polyfit(peakv(:,1),peakv(:,2),3);
stq_in = polyval(pfilt,time0719);

figure(10)
plot(time0719./60,stqin_av),hold on
plot(peakv(:,1)./60,peakv(:,2),'o','LineWidth',3)
```

```
% plot(time0719,stq_in,'--k','LineWidth',3)

legend('Inner Wall Strain','Peak Values')
set(gca,'FontSize',20)
xlabel('Time [Hours]')
ylabel('Strain [mm/mm]')
xlim([0 160])



t = time0719;

stq_out = zeros(1,size(t,2));

figure(3)
plot(time0719./60,stq1,'Color',[0    0.4470    0.7410],'LineWidth',0.5), hold on
plot(time0719./60,stq3,'Color',[0.8500    0.3250    0.0980],'LineWidth',0.5)
plot(t./60,stq_in,'k--','LineWidth',3)
plot(time0719./60,stq2,'Color',[0    0.4470    0.7410],'LineWidth',0.5)
plot(time0719./60,stq4,'Color',[0.8500    0.3250    0.0980],'LineWidth',0.5)
plot(t./60,stq_out,'k--','LineWidth',3)

legend('Inner Gauge','Outer Gauge','Line Fitting')
set(gca,'FontSize',20)
xlabel('Time [Hours]')
ylabel('Strain [mm/mm]')
xlim([0 160])

%% Pressure Plots
```

```
C = 0.1/0.000164;
Ro = 38.1;
Ri = 25.4;
r = Ri;

Pi = C.*stq_in;
Po = 0;

% Simulation result

simst = csvread('SimStrainResult.csv',1,0);
t_sim = simst(:,1)./60;
Pi_sim = C.*simst(:,2);

figure(5)
plot(t_sim./60,Pi_sim,'--','Color',[0.6350    0.0780    0.1840]...
    ,'LineWidth',3), hold on
plot(t./60,Pi,'LineWidth',3)

legend('Simulation','Experiment')
set(gca,'FontSize',20)
xlabel('Time [Hours]')
ylabel('Pressure [MPa]')
xlim([0 160])
```

```
%% Degree of Cure v P


doc = csvread('tdegofc.csv',1,0);

fitval = 18;
pdc = polyfit(doc(:,1),doc(:,2),fitval);

docp = polyval(pdc,t);
docs = polyval(pdc,t_sim);

figure(7)

plot(docs,Pi_sim,'--','Color',[0.6350    0.0780    0.1840]...
    ,'LineWidth',3), hold on
plot(docp,Pi,'LineWidth',3)

legend('Simulation','Experiment')
set(gca,'FontSize',20)
xlabel('Degree of Cure')
ylabel('Pressure [MPa]')


figure(8)
plot(doc(:,1),doc(:,2),'--','LineWidth',3), hold on
plot(t_sim,docs,'LineWidth',3)
```

```
legend('Simulation','Experiment')
set(gca,'FontSize',20)
xlabel('Time [Minutes]')
ylabel('Degree of Cure')

%% Temperature Fluctuation Analysis

flc = csvread('flc.csv',1,0);
h = flc(:,1);
qbfl = flc(:,2);



figure(9)
plot(time0719./60,stq1,'Color',[0    0.4470    0.7410],'LineWidth',1), hold on
%plot(h,qbfl,'--','Color',[0    0.4470    0.7410],'LineWidth',2)

plot(time0719./60,stq2,'Color',[0    0.4470    0.7410],'LineWidth',1)

%legend('Inner Gauge Experimental','Inner Gauge Simulation')
set(gca,'FontSize',20)
xlabel('Time [Hours]')
ylabel('Strain [mm/mm]')
xlim([0 160])



%% Components for New Bulk Modulus Estimation: mod = a.*exp(degcr) + c;
```

```
res = 0.03;

degc = [0 1];
lonM = [1000 2500];
shearM = [0 2500/2/(1+0.35)];
degcr = 0:res:1;

% FOLLOWING PARAMETERS WERE OBTAINED FROM CURVE FITTING APP ON MATLAB

aM = 18.75;
bM = 4.394;
cM = 981.3;
M = aM.*exp(bM.*degcr) + cM;

as = 11.57;
bs = 4.394;
cs = -11.57;
s = as.*exp(bs.*degcr) + cs;

% New Estimation

degc = [0 1];
lonM = [1000  2500];
shearM = [0 2500/2/(1+0.35)];
degcr = 0:res:1;


Mb = 7.314;
```

```
Mc = 999;
Ma = exp(Mb.*degcr) + Mc;


sb = 6.832;
sc = -1;
sa = exp(sb.*degcr) + sc;


% Last Bulk Modulus Estimation: mod = a.*exp(b.*degcr) + c;

degc = [0 0.5 1];
lonM = [1000 (2500-1000)/5+1000 2500];
shearM = [0 2500/2/(1+0.35)/5 2500/2/(1+0.35)];
degcr = 0:res:1;

Maf = 100;
Mbf = 2.773;
Mcf = 900;
FinM = Maf.*exp(Mbf.*degcr) + Mcf;

saf = 61.73;
sbf = 2.773;
scf = -61.73;
Fins = saf.*exp(sbf.*degcr) + scf;


figure(13)
```

```
plot(degcr,Ma,'--*','LineWidth',1.5,'Color',[0.4660    0.6740    0.1880]),...
hold on
plot(degcr,M,'--o','LineWidth',1.5,'Color',[0.4940    0.1840    0.5560])
plot(degcr,FinM,'--','LineWidth',1.5,'Color',[0.3010    0.7450    0.9330])

set(gca,'FontSize',20)
xlabel('Degree of Cure, \phi')
ylabel('Longitudinal Modulus, M [MPa]')
ylim([500 3000])
legend('Fitting 1','Fitting 2',' Fitting 3')

figure(14)
plot(degcr,sa,'--*','LineWidth',1.5,'Color',[0.4660    0.6740    0.1880]),...
hold on
plot(degcr,s,'--o','LineWidth',1.5,'Color',[0.4940    0.1840    0.5560])
plot(degcr,Fins,'--','LineWidth',1.5,'Color',[0.3010    0.7450    0.9330])

set(gca,'FontSize',20)
xlabel('Degree of Cure, \phi')
ylabel('Shear Modulus, \mu [MPa]')
ylim([0 1100])
legend('Fitting 1','Fitting 2',' Fitting 3')


%% Simulation Result Comparison

fit1 = csvread('fit1.csv',1,0);
```

```
fit2 = csvread('fit2.csv',1,0);
fit3 = csvread('fit3.csv',1,0);

t1 = fit1(:,1);
t2 = fit2(:,1);
t3 = fit3(:,1);

f1 = fit1(:,2);
f2 = fit2(:,2);
f3 = fit3(:,2);

figure(15)
plot(time0719./60,stq1,'Color',[0    0.4470    0.7410],'LineWidth',1), hold on
plot(t1,f1,'--','LineWidth',3,'Color',[0.4660    0.6740    0.1880])
plot(t2,f2,'--','LineWidth',3,'Color',[0.4940    0.1840    0.5560])
plot(t3,f3,'--','LineWidth',3,'Color',[0.3010    0.7450    0.9330])
plot(time0719./60,stq2,'Color',[0    0.4470    0.7410],'LineWidth',1)


set(gca,'FontSize',20)
xlabel('Time [hours]')
ylabel('Strain [mm/mm]')
legend('Experimental Result','Fitting 1','Fitting 2',' Fitting 3')


%% Temperature Change Analysis

alphAl = 2.*10.^(-5);
```

```
figure(16)
plot(time0719./60,(stq3+stq4)./alphAl./2,'Color',...
    [0.8500    0.3250    0.0980],'LineWidth',0.2), hold on

set(gca,'FontSize',20)
xlabel('Time [Hours]')
ylabel('Temperature [^{\circ}C]')
xlim([0 160])



%% Young's Modulus & Poisson's Ratio

% thstr = -stq_in(1:size(shr,1))*0.1857;


% str_r = C.*stq_in(1:size(shr,1)).*...
%        (1./Ro.^2 - 1./Ri.^2).*(1./Ro.^2 - 1./r.^2);
% str_th = C.*stq_in(1:size(shr,1)).*...
%        (1./Ro.^2 - 1./Ri.^2).*(1./Ro.^2 + 1./r.^2);

%
% str_r = -Po - (Pi - Po).*(Ri.^2).*(r.^2 - Ro.^2)...
%       ./(r.^2)./((Ri).^2-Ro.^2);
% str_th = -Po - (Pi - Po).*(Ri.^2).*(r.^2 + Ro.^2)...
%       ./(r.^2)./((Ri).^2-Ro.^2);
%
```

```
%
% E = (thstr./str_th -(str_r.*zstr)./(str_th.*(str_th+str_r))).^-1;
%
% figure(5)
% plot(t,E)
%
```